STAMBPL1 activates the GRHL3/HIF1A/VEGFA axis through interaction with FOXO1 to promote angiogenesis in triple-negative breast cancer

Huan Fang[1,2#], Huichun Liang[1#], Chuanyu Yang[1], Dewei Jiang[1], Qianmei Luo[1], Wenming Cao[3*], Huifeng Zhang[4*], Ceshi Chen[5,6,1*]

1. Kunming Institute of Zoology, Chinese Academy of Sciences, Kunming, Yunnan, China.

2. Kunming College of Life Sciences, University of Chinese Academy of Sciences, Kunming, Yunnan, China.

3. The Department of Breast Medical Oncology, Zhejiang Cancer Hospital, Hangzhou 310022, China.

4. Department of Pharmacy, the First People's Hospital of Yunnan Province/the Affiliated Hospital of Kunming University of Science and Technology, Kunming, Yunnan Province, China

5. Academy of Biomedical Engineering, Kunming Medical University, Kunming 650500, China.

6. The Third Affiliated Hospital, Kunming Medical University, Kunming 650118, China.

# These authors contributed equally to this work.

* Corresponding authors: Wenming Cao, E-mail: caowm@zjcc.org.cn; Huifeng Zhang, E-mail: zhanghuifeng92@163.com; or Ceshi Chen, E-mail: chenc@kmmu.edu.cn.

Abstract

In the clinic, anti-tumor angiogenesis is commonly employed for treating recurrent, metastatic, drug-resistant triple-negative and advanced breast cancer. Our previous research revealed that the deubiquitinase STAMBPL1 enhances the stability of MKP-1, thereby promoting cisplatin resistance in breast cancer. In this study, we discovered that STAMBPL1 could upregulate the expression of the hypoxia-inducible factor HIF1α in breast cancer cells. Therefore, we investigated whether STAMBPL1 promotes tumor angiogenesis. We demonstrated that STAMBPL1 increased *HIF1A* transcription in a non-enzymatic manner, thereby activating the HIF1α/VEGFA signaling pathway to facilitate TNBC angiogenesis. Through RNA-seq analysis, we identified the transcription factor GRHL3 as a downstream target of STAMBPL1 that is responsible for mediating *HIF1A* transcription. Furthermore, we discovered that STAMBPL1 regulates *GRHL3* transcription by interacting with the transcription factor FOXO1. These findings shed light on the role and mechanism of STAMBPL1 in the pathogenesis of breast cancer, offering novel targets and avenues for the treatment of triple-negative and advanced breast cancer.

Keywords Triple-negative breast cancer, tumor angiogenesis, transcription regulation

Introduction

Triple-negative breast cancer (TNBC) is a subtype of breast cancer characterized by a lack of expression of estrogen receptor (ER), progesterone receptor (PR), and human epidermal growth factor receptor 2 (HER2). Despite representing only 10–15% of all breast cancer cases, it is associated with a greater risk of recurrence, metastasis, and resistance to chemotherapy, leading to a poorer prognosis than other types of breast cancer[1]. Therefore, understanding the pathogenesis of this subtype of breast cancer and identifying effective treatment targets are key areas of research focus and challenge. In the clinic, in addition to surgery, radiotherapy, and chemotherapy, treatment approaches for TNBC also include the use of epidermal growth factor receptor (EGFR) inhibitors, poly (ADP-ribose) polymerase (PARP) inhibitors, immune checkpoint inhibitors, and anti-angiogenic therapies[2,3].

For solid tumors, the survival, proliferation, and invasion of cancer cells rely on surrounding blood vessels to provide nutrients and oxygen. Cancer cells can increase the synthesis and secretion of the vascular endothelial growth factor A (VEGFA), activate endothelial cells in neighboring blood vessels through paracrine pathways, and stimulate tumor angiogenesis[4]. Therefore, investigating the upstream molecular mechanisms that activate VEGFA in cancer cells offers new targets for inhibiting TNBC angiogenesis via disruption of this signaling pathway.

The deubiquitinase STAMBPL1 (also known as AMSH-LP) belongs to the AMSH family and cleaves K63-linked polyubiquitin chains[5]. STAMBPL1 stabilizes XIAP to inhibit apoptosis in prostate cancer cells[6] and confers resistance to honokiol-induced apoptosis in various cancer cell types by stabilizing Survivin and c-FLIP[7]. Our previous research demonstrated that

57 STAMBPL1 enhances cisplatin resistance in TNBC cells through the stabilization of MKP-1[8].
58 In this study, we discovered that, independent of its deubiquitinating enzyme activity,
59 STAMBPL1 upregulates HIF1α expression in TNBC cells. We aimed to investigate the
60 molecular mechanism by which it upregulates HIF1α and explore its role in tumor
61 angiogenesis in TNBC.
62 FOXO1, a member of the forkhead box transcription factor family, regulates various
63 physiological and pathological processes, such as cell proliferation, apoptosis, autophagy,
64 and oxidative stress[9]. In breast cancer, FOXO1 enhances the stemness of cancer cells by
65 promoting *SOX2* transcription[10] and confers resistance to chemotherapy drugs in basal-like
66 breast cancer cells by activating *KLF5* transcription[11]. Furthermore, FOXO1 plays a crucial
67 role in angiogenesis by upregulating VEGFA transcription[12]. However, the specific mechanism
68 by which FOXO1 regulates VEGFA transcription remains unclear, and its role in tumor
69 angiogenesis in TNBC requires further investigation.
70 In this study, we discovered that STAMBPL1 facilitates the transcriptional regulation of
71 *GRHL3* by interacting with FOXO1, consequently enhancing *HIF1A* transcription through
72 GRHL3 to activate the HIF1α/VEGFA pathway. This results in increased endothelial cell
73 activity via paracrine signaling, thereby promoting tumor angiogenesis in TNBC.
74

Methods

Cell lines and reagents

All cell lines used in this study, including HCC1806, HCC1937, and HEK293T cells, were purchased from ATCC (American Type Culture Collection, Manassas, VA, USA) and validated by short tandem repeat (STR) analysis, and these cell lines tested negative for mycoplasma contamination. HCC1806 and HCC1937 cells were cultured in RPMI 1640 medium supplemented with 5% FBS. HEK293T cells were cultured in DMEM (Thermo Fisher, Grand Island, USA) with 5% FBS at 37°C with 5% CO_2. Primary human umbilical vein endothelial cells (HUVECs) were maintained in an EGM-2 Bullet Kit (CC-3162, Lonza, USA). AS1842856 (Cat#HY-100596) and apatinib (Cat#HY-13342S) were purchased from MCE (New Jersey, USA).

Plasmid construction and stable STAMBPL1, GRHL3 and FOXO1 overexpression

We constructed the full-length *STAMBPL1/GRHL3/FOXO1* genes and then subcloned them into the pCDH lentiviral vector. The packaging plasmids (pMDLg/pRRE, pRSV-Rev, and pCMV-VSV-G) and the pCDH-STAMBPL1/GRHL3/FOXO1 expression plasmid were cotransfected into HEK293T cells (2×10^6 in 10 cm plates) to produce lentiviruses. Following transfection for 48 hours, the lentivirus was collected and used to infect HCC1806 and HCC1937 cells. Forty-eight hours later, puromycin (2 μg/ml) was used to screen the cell populations.

Stable knockdown of STAMBPL1 and GRHL3

The pSIH1-H1-puro shRNA vector was used to express STAMBPL1, GRHL3 and luciferase (LUC) shRNAs. *STAMBPL1* shRNA#1, 5'-GGAGCATCAGAGATTGATA-3'; *STAMBPL1*

shRNA#2, 5'-GCTGCTATGCCTGACCATA-3'; *GRHL3* shRNA#1, 5'-CCTTGAGCTTCCTCTATGA-3'; *GRHL3* shRNA#2, 5'-AGAGGAAGATGCGCGATGA-3'; *Luciferase* shRNA, 5'-CUUACGCUGAGUACUUCGA-3'; HCC1806 and HCC1937 cells were infected with lentivirus. Stable populations were selected via the use of 1 to 2 mg/mL puromycin. The knockdown effect was evaluated by Western blotting.

RNA interference

The siRNA target sequences used in this study were as follows: *STAMBPL1* siRNA#1, 5'-GGAGCATCAGAGATTGATA-3'; *STAMBPL1* siRNA#2, 5'-GCTGCTATGCCTGACCATA-3'; *GRHL3* siRNA#1, 5'-CCTTGAGCTTCCTCTATGA-3'; *GRHL3* siRNA#2, 5'-AGAGGAAGATGCGCGATGA-3'; *HIF1α* siRNA#1, 5'-AAGAGGTGGATATGTCTGG-3'; *HIF1α* siRNA#2, 5'-CGTCGAAAAGAAAAGTCTCTT-3'; *FOXO1* siRNA#1, 5'-CCCAGAUGCCUAUACAAAC-3'; and *FOXO1* siRNA#2, 5'-CTCAAATGCTAGTACTATTAG-3'. All siRNAs were synthesized by RiboBio (RiboBio, China) and transfected at a final concentration of 50 nM.

Western blotting (WB) and antibodies

The WB procedure was described in our previous study[13]. Anti-STAMBPL1 (sc-376526) and anti-GAPDH (sc-25778) antibodies were purchased from Santa Cruz Biotechnology (Santa Cruz, CA, USA). Anti-FOXO1 (#2880S) and anti-HIF1α (#36169S) antibodies were purchased from CST. Anti-β-actin (A5441) and anti-GST (G7781) antibodies were purchased from Sigma–Aldrich (St. Louis, MO, USA). The anti-Flag (ab205606) antibody was purchased from Abcam.

Real-time polymerase chain reaction (RT–qPCR)

Total RNA was extracted via TRIzol (Invitrogen, 15596026). One microgram of total RNA was reverse transcribed to cDNA according to the manufacturer's instructions for the HiScript II QRT SuperMix for qPCR Kit (Vazyme, R223-01). For quantitative PCR (RT–qPCR), the SYBR Green Select Master Mix system (Applied Biosystems, 4472908, USA) was used on an ABI-7900HT system (Applied Biosystems, 4351405). The primers used for PCR were as follows: 18S forward, 5′-CTCAACACGGGAAACCTCAC-3′; 18S reverse, 5′-CGCTCCACCAACTAAGAACG-3′; HIF1α forward, 5′-AAGTCTGCAACATGGAAGGTAT-3′; HIF1α reverse, 5′-TGAGGAATGGGTTCACAAATC-3′; VEGFA forward, 5′-TGAGGAATGGGTTCACAAATC-3′; VEGFA reverse, 5′-ATCTGCATGGTGATGTTGGA-3′; GLUT1 forward, 5′-TCGTCGGCATCCTCATCGCC-3′; GLUT1 reverse, 5′-CCGGTTCTCCTCGTTGCGGT-3′; GRHL3 forward, 5′-GGGGCTGAGGAATGCGATCT-3′; and GRHL3 reverse, 5′-AATTTTGCCGTCCAGCTCCC-3′.

Cell proliferation and migration assays

To detect the proliferation of HUVECs, we used the Click-iT™ EdU Alexa Fluor™ 647 Imaging Kit (Invitrogen) according to the manufacturer’s protocol. Briefly, HUVECs were seeded on coverslips (BD Biosciences) at 0.5×10^5 cells per well. The next day, the supernatants were discarded, and the cells were cultured with conditioned medium (CM). Six hours later, the cells were incubated with EdU in CM for 4 hours, followed by fixation and staining. For each sample, three random fields were observed via fluorescence microscopy, and the total numbers of cells and EdU-positive cells were counted. To detect the migration of HUVECs, we performed a wound-healing assay. Twenty-four hours after seeding, the supernatants of the HUVECs were discarded, and the cells were scratched and cultured with CM for 24 hours.

141 Wound closure was imaged via microscopy. For each image, the gap width was analyzed via
142 ImageJ.

143 **Tube formation assays**

144 HUVECs (1×10^4) in CM were seeded onto Matrigel (BD Biosciences)-coated μ-Slide
145 angiogenesis plates (ibidiGmbH, Munich, Germany). At 6 hours after seeding, images were
146 taken via microscopy and then analyzed with ImageJ. The total branch length was measured.

147 **Chromatin immunoprecipitation assays**

148 After the sample preparation was completed, the subsequent experimental steps were
149 performed according to the instructions of the Simple ChIP (R) Plus Kit (CST, # 9005). The
150 PCR primers for amplifying the region of interest on the HIF1α gene promoter were as
151 follows: 5′-GACTGACAGGCTTGAAGTTTATGC-3′ and 5′-
152 TGTTGCTGTAAACTTCAAGGGAAA-3′, and the PCR primers for amplifying the region of
153 interest on the GRHL3 gene promoter were as follows: 5′-TTCTATCCCTTCTGTGCTGACCA-
154 3′ and 5′-TGTGCCAGACCCTACTCTGGG-3′.

155 **Dual-luciferase reporter assays**

156 The DNA fragments HIF1α and GRHL3 were amplified from MCF10A cell genomic DNA via
157 PCR template and then cloned and inserted into the pGL3-Basic vector. HEK293T cells were
158 seeded in 24-well plates and transfected with pCDH-GRHL3-3×Flag or pCDH-FOXO1-3×Flag
159 and pGL3 luciferase reporter plasmids (both 600 ng/well) together with the pCMV-Renilla
160 control (5 ng/well). After transfection for 48 h, the cell lysates were collected, and the
161 luciferase activities were detected via the dual-luciferase reporter assay system (Promega,
162 USA). For the WT HIF1α promoter (with the GRHL3 binding motif), the primers used for PCR

163 were as follows: forward, 5′-gctagcccgggctcgagatctCCACTGCGCTCCAGCCTG-3′; reverse,
164 5′-cagtaccggaatgccaagcttCCTCAGACGAGGCAGCACTG-3′. For the mutant HIF1α promoter
165 (without the GRHL3 binding motif), the primers used for PCR were as follows: forward, 5′-
166 TCTTTCCCTGAGGCCTTCCTATATGCTTAT-3′; reverse, 5′-
167 ATAAGCATATAGGAAGGCCTCAGGGAAAGA-3′. For the WT GRHL3 promoter (with the
168 FOXO1 binding motif), the primers used for PCR were as follows: forward, 5′-
169 gctagcccgggctcgagatctATTAACAAGGGTGACTGAAGAGGG-3′; reverse, 5′-
170 cagtaccggaatgccaagcttTGGAGGTATACCTCAACAGGTGC-3′. For the mutant GRHL3
171 promoter (without the FOXO1 binding motif), the primers used for PCR were as follows:
172 forward, 5′-CTCCCCCACCAAACAAAGAAGGAGAACACCCC-3′; reverse, 5′-
173 GGGGTGTTCTCCTTCTTTGTTTGGTGGGGGAG-3′.

174 **Immunofluorescence staining**

175 HEK293T cells plated on cell culture slides were transfected with the STAMBPL1 and FOXO1
176 expression plasmids. Two days after transfection, the cells were fixed in 3.7%
177 polyformaldehyde at 4°C overnight. After being blocked with 5% BSA at room temperature for
178 1 hour, the cells were stained with anti-STAMBPL1 (mouse) and anti-FOXO1 (rabbit)
179 antibodies at 4°C overnight. The cells were subsequently stained with both an Alexa
180 Fluor647-labeled anti-mouse secondary antibody and a FITC-labeled anti-rabbit secondary
181 antibody (ZSGB-Bio, Beijing, China) at room temperature for 1 hour. Nuclei were stained with
182 DAPI (Biosharp, BL739A) for 15 min. Images were captured via a confocal microscope.

183 **Immunoprecipitation and GST pull-down**

184 For endogenous protein interaction, cell lysates were first incubated with anti-FOXO1

185 antibodies or rabbit IgG (2729S; Cell Signaling Technology) and then incubated with protein
186 A/G magnetic beads (HY-K0202; MCE). For the GST pull-down assay, the cell lysates were
187 directly incubated with Glutathione Sepharose 4B (10312185; Cytiva) overnight at 4°C. For
188 the IP-Flag assay, cell lysates were directly incubated with anti-Flag magnetic beads (HY-
189 K0207; MCE) overnight at 4°C. The precipitates were washed four times with 1 ml of lysis
190 buffer, boiled for 10 minutes with 1×SDS sample buffer, and subjected to WB analysis.

191 **Xenograft experiments**

192 We purchased 5- to 6-week-old female BALB/c nude mice from SLACCAS (Changsha,
193 China). Animal feeding and experiments were approved by the animal ethics committee of
194 Kunming Institute of Zoology, Chinese Academy of Sciences. HCC1806-shLuc, HCC1806-
195 shSTAMBPL1, or HCC1806-shGRHL3 cells and HCC1806-PCDH-Vector or HCC1806-
196 PCDH-STAMBPL1 cells (1×10^6 in Matrigel (BD Biosciences, NY, USA)) were implanted into
197 the mammary fat pads of the mice. When the tumor volume reached approximately 50 mm^3,
198 the nude mice were randomly assigned to the control or treatment groups (n = 4/group). The
199 control group was given vehicle alone, and the treatment group received the FOXO1 inhibitor
200 AS1842856 (10 mg/kg), the VEGFR inhibitor apatinib (50 mg/kg), and the FOXO1 inhibitor
201 AS1842856 combined with the VEGFR inhibitor apatinib via intragastric administration every
202 two days for 20 days. The tumor volume was calculated as follows: tumor volume was
203 calculated by the formula ($\pi \times$ length $\times$ width^2)/6. The maximal tumor size permitted by the
204 animal ethics committee of Kunming Institute of Zoology, Chinese Academy of Sciences, and
205 the maximal tumor size in this study was not exceeded.

206 **Immunohistochemical staining**

The xenograft tumor tissues were fixed in 3.7% formalin solution. The immunohistochemistry was performed on 4-μm-thick paraffin sections after pressure-cooking for antigen retrieval. An anti-CD31 primary antibody (1:400, Abcam, ab28364) was used. After 12 h, the slides were washed three times with PBS and incubated with secondary antibodies (hypersensitive enzyme-labeled goat anti-mouse/rabbit IgG polymer (OriGene, China) at room temperature for 20 min, DAB concentrated chromogenic solution (1:200 dilution of concentrated DAB chromogenic solution)), counterstained with 0.5% hematoxylin, dehydrated with graded concentrations of ethanol for 3 min each (70%–80%–90%–100%), and finally stained with dimethyl benzene. The immunostained slides were evaluated via light microscopy, and the number of microvessels with positive CD31 expression was counted.

Statistical analysis

All the graphs were created via GraphPad Prism software version 8.0. Comparisons between two independent groups were assessed via two-tailed Student's *t* tests. One-way analysis of variance with least significant differences was used for multiple group comparisons. *P* values of < 0.05, 0.01 or 0.001 were considered to indicate statistically significant results, and comparisons that were significant at the 0.05 level are indicated by *, those at the 0.01 level are indicated by **, and those at the 0.001 level are indicated by ***.

225 **Results**

226 **STAMBPL1 upregulates HIF1α in a non-enzymatic manner in TNBC cells.**

227 Our previous research revealed that STAMBPL1, a deubiquitinase, promotes cisplatin
228 resistance in TNBC by stabilizing MKP1[8]. To further investigate the role and mechanism of
229 STAMBPL1 in TNBC, we discovered that the knockdown of STAMBPL1 can inhibit hypoxia-
230 induced HIF1α expression (Fig. 1A) and suppress the transcription of the HIF1α downstream
231 genes *VEGFA* and *GLUT1* (Fig. 1B-E). Under normoxic conditions, both STAMBPL1 and its
232 enzymatically mutated variant (E292A) can upregulate the protein expression of HIF1α (Fig.
233 1F). These findings suggest that STAMBPL1 enhances the expression of HIF1α in breast
234 cancer cells through a non-DUB enzyme activity mechanism.

235 **STAMBPL1 promotes *HIF1A* transcription and activates the HIF1α/VEGFA axis.**

236 To elucidate how STAMBPL1 upregulates HIF1α, we examined the transcription levels of
237 *HIF1A*. These results indicate that knocking down STAMBPL1 significantly inhibits the
238 transcription of *HIF1A* (Fig. 2A-C). STAMBPL1 overexpression increased the transcription of
239 *HIF1A* (Fig. 4E and SFig. 3E) and *VEGFA* (Fig. 2E and 2G). The ability of STAMBPL1 to
240 induce *VEGFA* transcription was blocked by HIF1α knockdown (Fig. 2D-G). These findings
241 suggested that STAMBPL1 activated the HIF1α/VEGFA axis through enhancing the
242 transcription of *HIF1α*.

243 **STAMBPL1 in TNBC cells enhances the activity of HUVECs and promotes TNBC**
244 **angiogenesis.**

245 The conditioned medium (CM) from TNBC cells with STAMBPL1 knockdown inhibited the

246 proliferation (Fig. 3A-B, and SFig. 1A-B), migration (Fig. 3C-D, and SFig. 1C-D), and tube
247 formation (Fig. 3E-F, and SFig. 1E-F) of HUVECs. When STAMBPL1 was overexpressed in
248 TNBC cells, the conditioned medium of HCC1806 and HCC1937 cells promoted the ability of
249 HUVECs to proliferate (SFig. 2A and 2D), migrate (SFig. 2B and 2E), and form tubes (SFig.
250 2C and 2F), which could be reversed by knocking down HIF1α in TNBC cells. These findings
251 suggest that STAMBPL1 activates the HIF1α/VEGFA axis in TNBC cells, leading to enhanced
252 abilities of HUVECs through a paracrine pathway. Knocking down STAMBPL1 inhibited the
253 growth of HCC1806 xenografts in mice (Fig. 3G-I) and decreased the number of microvessels
254 in tumor tissue (Fig. 3J-K), indicating that STAMBPL1 promoted tumor angiogenesis.

255 **STAMBPL1 promotes *HIF1A* transcription via the upregulation of GRHL3.**

256 By silencing the *STAMBPL1* gene in HCC1806 cells subjected to 10 hours of hypoxia, we
257 performed RNA-seq analysis to investigate the mechanism by which STAMBPL1 promotes
258 *HIF1A* transcription. We found that silencing of STAMBPL1 resulted in the downregulation of
259 27 genes (of which only 18 were annotated), with *GRHL3* being the sole gene encoding a
260 transcription factor (Fig. 4A and SFig. 3A). Silencing of STAMBPL1 inhibited *GRHL3*
261 transcription in both HCC1806 and HCC1937 cells (Fig. 4B and SFig. 3B). Conversely, the
262 overexpression of STAMBPL1 promoted *GRHL3* transcription (Fig. 4D and SFig. 3D).
263 Furthermore, the stimulatory effects of STAMBPL1 on the HIF1α/VEGFA axis (Fig. 4C-F and
264 SFig. 3C-F) and on HUVECs (Fig. 4G-I and SFig. 3G-I) were reversed by GRHL3 knockdown.
265 These findings suggest that STAMBPL1 activates the HIF1α/VEGFA axis by upregulating
266 GRHL3.

267 **GRHL3 enhances *HIF1A* transcription by binding to its promoter.**

268 On the basis of the GRHL binding motif (Fig. 5A), a GRHL binding sequence was identified in
269 the *HIF1A* promoter (Fig. 5B). ChIP and luciferase assays revealed that GRHL3 bound to the
270 *HIF1A* promoter (Fig. 5D) and increased its activity (Fig. 5E). Knockdown of GRHL3 (Fig. 5G
271 and SFig. 4B) resulted in decreased expression of HIF1α at both the mRNA (Fig. 5H and
272 SFig. 4C) and protein levels (Fig. 5F and SFig. 4A), leading to suppressed *VEGFA*
273 transcription (Fig. 5I and SFig. 4D), indicating that GRHL3 promotes *HIF1A* transcription by
274 binding to its promoter.
275 Furthermore, conditioned medium from TNBC cells with GRHL3 knockdown inhibited HUVEC
276 proliferation, migration, and tube formation (Fig. 5J-L and SFig. 4E-G). The overexpression of
277 GRHL3 in TNBC cells activated the HIF1α/VEGFA axis (Fig. 6A-B and SFig. 4H-J), resulting
278 in increased proliferation, migration, and tube formation in HUVECs. This effect was reversed
279 by knocking down HIF1α in TNBC cells (Fig. 6C-E and SFig. 4K-M). Knockdown of GRHL3
280 (Fig. 6F) also inhibited tumor growth in HCC1806 xenograft mice (Fig. 6G-I) and reduced the
281 number of microvessels in tumor tissues (Fig. 6J-K).

282 **STAMBPL1 mediates *GRHL3* transcription by interacting with FOXO1.**

283 Our previous study demonstrated that STAMBPL1 is localized in the nucleus[8]. This protein
284 may promote the transcription of GRHL3 through interactions with other transcription factors.
285 Previous studies have indicated that FOXO1 acts as an upstream transcription factor of
286 GRHL3[14]. Therefore, we aimed to investigate whether STAMBPL1 promotes GRHL3
287 transcription via FOXO1. Our experimental data revealed that knockdown of FOXO1 in TNBC
288 cells not only inhibited the GRHL3/HIF1α/VEGFA axis (Fig. 7A-D and SFig. 5A-D) but also
289 reversed the stimulatory effects of STAMBPL1 on this axis (Fig. 7E-H and SFig. 5E-H).

290 Furthermore, FOXO1 was found to bind to the promoter region of GRHL3 (Fig. 7I and SFig.
291 5I) and enhance its transcriptional activity (Fig. 7J). STAMBPL1 was shown to increase the
292 transcriptional activation of FOXO1 at the GRHL3 promoter (Fig. 7K), and it also bound to the
293 GRHL3 promoter; however, this interaction could be disrupted by FOXO1 knockdown (Fig.
294 7L).
295 To investigate the mechanism by which STAMBPL1 promotes GRHL3 transcription through
296 FOXO1, we conducted immunofluorescence and immunoprecipitation assays. We observed
297 the colocalization of STAMBPL1 and FOXO1 in the nucleus (Fig. 7M) and identified an
298 interaction between them in HCC1937 cells (Fig. 7N). Through the generation of a series of
299 Flag-FOXO1/GST-fused STAMBPL1 deletion mutants, we mapped the regions of the proteins
300 responsible for this interaction (SFig. 5F–G). The results of the GST pulldown assay indicated
301 that the N-terminus (1–140 aa) of STAMBPL1 interacted with FOXO1 (SFig. 5H). Additionally,
302 an immunoprecipitation assay revealed an interaction between the FOXO1 protein (250–596
303 aa) and STAMBPL1 (SFig. 5I). These findings suggest that STAMBPL1 promotes GRHL3
304 transcription by interacting with FOXO1.

305 **The combination of VEGFR and FOXO1 inhibitors synergistically suppresses TNBC**
306 **xenograft growth.**

307 Through analysis of the TCGA database, we determined that *STAMBPL1*, *FOXO1*, and
308 *GRHL3* exhibited high expression levels in TNBC tumors compared with non-TNBC tumors
309 (Fig. 8A-C). To assess the potential therapeutic efficacy of cotreatment with the FOXO1
310 inhibitor AS1842856 and the VEGFR inhibitor apatinib *in vivo*, we conducted animal
311 experiments in nude mice. HCC1806 cells overexpressing STAMBPL1 were orthotopically

312 implanted into the mammary fat pads of 6-week-old female mice (n=16/group). Once the
313 tumor volume reached approximately 50 mm^3, the mice were divided into four subgroups to
314 receive apatinib (50 mg/kg, once every two days), AS1842856 (10 mg/kg, once every two
315 days), a combination of both drugs, or vehicle control for 20 days. Our findings indicated that
316 STAMBPL1 overexpression enhanced breast cancer cell growth *in vivo*. While the individual
317 inhibitory effects of the FOXO1 and VEGFR inhibitors on tumor growth were not significant,
318 the combined treatment markedly suppressed tumor growth in nude mice (Fig. 8E-G).
319 Importantly, the drug treatments did not affect the body weights of the mice (Fig. 8H). These
320 results suggest that the combined administration of AS1842856 and apatinib effectively
321 inhibits tumor growth in nude mice.
322

Discussion

In this study, we discovered that STAMBPL1 promotes angiogenesis in TNBC by activating the HIF1α/VEGFA pathway independently of its enzymatic activity. Through RNA-seq analysis, we revealed that STAMBPL1 positively regulates the transcription of *GRHL3*. Furthermore, we demonstrated that GRHL3 binds to the promoter of the *HIF1A* gene, thereby increasing its transcription. Additionally, we found that STAMBPL1 interacts with FOXO1 to facilitate the transcription of GRHL3/HIF1α/VEGFA. Importantly, we confirmed that the combination of the FOXO1 inhibitor AS1842856 and the VEGFR inhibitor apatinib effectively inhibited tumor growth in nude mice. These findings suggest that both STAMBPL1 and FOXO1 may be potential therapeutic targets for inhibiting angiogenesis in TNBC. This study is the first to uncover the role of STAMBPL1 in promoting angiogenesis through the FOXO1/GRHL3/HIF1α axis. Furthermore, a novel transcription factor, GRHL3, which regulates the transcription of HIF1α, was identified. These findings provide valuable insights for developing new therapeutic strategies to target TNBC.

The role of STAMBPL1 in tumors has not been fully recognized. Recent studies have reported its involvement in the epithelial–mesenchymal transition of various cancers, and its absence has been shown to affect the mesenchymal phenotype of lung and breast cancer[15]. Our previous research demonstrated that STAMBPL1 can stabilize MKP1 through deubiquitination and that the deletion of STAMBPL1 and MKP1 increases the sensitivity of breast cancer cells to cisplatin[16], suggesting that STAMBPL1 may be a potential therapeutic target for breast cancer. However, the mechanism by which STAMBPL1 activates the transcriptional activity of FOXO1 has not been elucidated, as STAMBPL1 does not stabilize the FOXO1 protein

345 through its deubiquitinating enzyme activity. We speculate that STAMBPL1 may recruit other
346 coactivators to FOXO1 transcription complexes. It will be important to develop a *Stambpl1*
347 knockout mouse model to investigate the exact role of STAMBPL1 in TNBC. Additionally, we
348 need to develop HIF1α and FOXO1 antibodies suitable for immunohistochemistry to detect
349 their expression in TNBC clinical samples.

350 Several studies have reported that FOXO1 inhibits tumor angiogenesis[17-21]. Studies have
351 shown that M2 macrophage-derived exosomal miR-942 promotes the migration and invasion
352 of lung adenocarcinoma cells and facilitates angiogenesis by binding to FOXO1 to alleviate
353 the inhibition of β-catenin, in which the upregulation of FOXO1 induces a decrease in cell
354 invasion and angiogenesis *in vitro*[17]. FOXO1 inhibits gastric cancer growth and angiogenesis
355 under hypoxic conditions via inactivation of the HIF1α-VEGF pathway, possibly in association
356 with SIRT1[18]. Cancer-associated fibroblast (CAF)-derived extracellular vesicles (EVs) deliver
357 miR-135b-5p into colorectal adenocarcinoma cells to downregulate FOXO1 and promote
358 HUVEC proliferation, migration, and angiogenesis[19]. Colorectal cancer cell-derived exosomes
359 overexpressing miR-183-5p promote the proliferation, migration and tube formation of HMEC-
360 1 (human microvascular endothelial cells) cells through the inhibition of FOXO1[20]. Bladder
361 cancer cell-derived exosomal miR-1247-3p facilitates angiogenesis by inhibiting FOXO1
362 expression[21]. However, the role of FOXO1 in breast cancer angiogenesis has not been
363 studied, and our study revealed that FOXO1 can promote the expression of HIF1α and
364 VEGFA, suggesting that it may play a role in promoting angiogenesis in breast cancer.

365 Studies have demonstrated that the AKT–FOXO1 signaling pathway regulates the expression

366 of GRHL3. To investigate this, the researchers utilized a previously published ChIP-seq
367 dataset for FOXO1 from human endometrial stromal cells. They reported that FOXO1
368 occupied BRD4-bound enhancers near the *GRHL3* gene. The authors subsequently
369 confirmed that the removal of EGF and insulin from the growth medium significantly increased
370 the expression of GRHL3, but the administration of the FOXO1 inhibitor AS1842856 partially
371 blocked the induced expression of GRHL3[14]. These results suggest that FOXO1 plays a
372 regulatory role upstream of GRHL3, and our study also confirmed that FOXO1 promotes the
373 transcription of *GRHL3* by binding to its promoter.

374 GRHL3 is a highly conserved epidermal-specific developmental transcription factor that has
375 recently gained attention in the field of cancer research[22]. To date, only a few genes regulated
376 by GRHL3 have been identified. Studies have shown that GRHL3 levels are significantly
377 reduced in human skin and head and neck squamous cell carcinomas and suggest that
378 GRHL3 is a key tumor suppressor pathway in squamous cell carcinomas[23]. GRHL3 was also
379 found to be induced by TNF-α in the mammary carcinoma cell line MCF-7 and was identified
380 as a TNFα-induced endothelial cell migration factor with promigratory activity as high as that
381 of VEGF[24]. However, the specific role of GRHL3 in breast cancer is unclear. Studies have
382 confirmed that GRHL3 strongly stimulates endothelial cell migration, which is consistent with
383 an angiogenic, protumorigenic function[24]. In our study, we demonstrated that GRHL3
384 promotes TNBC angiogenesis. HIF1α, a known regulator of angiogenesis, is regulated by
385 growth factors[25,26], cytokines[27] and mitogens[28,29]. The EGFR/Akt pathway is a known positive
386 regulator of HIF1α, potentially through mTOR[25] or independent of it[30,31]. While the
387 mechanisms regulating HIFα protein expression have been extensively studied, those

388 modulating HIF1α transcriptional activity remain unclear. Our study reveals for the first time
389 that GRHL3 promotes transcriptional activity by binding to the promoter of the *HIF1α* gene.

390 **Conclusions**

391 In summary, STAMBPL1 promoted TNBC angiogenesis by activating the GRHL3/HIF1A
392 pathway via FOXO1 in a non-enzymatic manner. These findings highlight the significant role
393 of STAMBPL1 in TNBC angiogenesis and suggest that targeting the
394 STAMBL1/FOXO1/GRHL3/HIF1α/VEGFA axis could be a potential therapeutic strategy to
395 inhibit angiogenesis in TNBC.

396 **List of abbreviations**

397 TNBC: triple-negative breast cancer

398 ER: estrogen receptor

399 PR: progesterone receptor

400 HER2: human epidermal growth factor receptor 2

401 EGFR: epidermal growth factor receptor

402 PARP: poly (ADP-ribose) polymerase

403 VEGFA: vascular endothelial growth factor A

404 HUVECs: primary human umbilical vein endothelial cells

405 CM: conditioned medium

406 **Supplementary information**

407 Supplementary Data (Supplementary Material 1) are available at JECCR Online.

408 **Acknowledgements**

409 We sincerely thank the team members for their dedication to this study.

Authors' contributions

Ceshi Chen, Huifeng Zhang, Wenmin Cao and Huichun Liang: conceptualization; Huan Fang, Huichun Liang and Ceshi Chen: data curation; Huan Fang and Huichun Liang: formal analysis, methodology and writing-original draft with help from Chuanyu Yang, Dewei Jiang and Qianmei Luo; Ceshi Chen, Huichun Liang, Huifeng Zhang, and Wenmin Cao: funding acquisition, project administration, validation, supervision and writing-review & editing.

Funding

This work was supported by National Key Research and Development Program of China (2023YFA1800500, 2020YFA0112300), National Natural Science Foundation of China (U2102203 to CC, 82203413 to HL), Biomedical Projects of Yunnan Key Science and Technology Program (202302AA310046 to CC), Yunnan Fundamental Research Projects (202301AS070050 to CC, 202201AT070290 to HL), Yunnan Revitalization Talent Support Program (Yunling Shcolar Project to CC), Yunnan (Kunming) Academician Expert Workstation (grant No. YSZJGZZ-2020025 to CC), Kunming University of Science and Technology-The First People's Hospital of Yunnan Province Joint Major Project (No. KUST-KH2022005Z), and Center of Clinical Pharmacy of the First People's Hospital of Yunnan Province Open Project (No. 2023YJZX-YX04).

Declarations

Ethics approval and consent to participate

All experimental procedures involving animals were performed in accordance to the Animal Welfare Law of China and the Guidelines for Animal Experiment of Kunming Institute of Zoology, Chinese Academy of Sciences.

432 **Consent for publication**

433 Not applicable.

434 **Availability of data and materials**

435 The datasets used and/or analyzed during the current study are available from the

436 corresponding author on reasonable request.

437 **Competing interests**

438 The authors declare that they have no conflicts of interest.

439 **References**

440 1. Geyer, F.C., Pareja, F., Weigelt, B., Rakha, E., Ellis, I.O., Schnitt, S.J., and Reis-Filho, J.S.
441 (2017). The Spectrum of Triple-Negative Breast Disease: High- and Low-Grade Lesions.
442 Am J Pathol *187*, 2139-2151. 10.1016/j.ajpath.2017.03.016.
443 2. Zagami, P., and Carey, L.A. (2022). Triple negative breast cancer: Pitfalls and progress.
444 NPJ Breast Cancer *8*, 95. 10.1038/s41523-022-00468-0.
445 3. Garcia, J., Hurwitz, H.I., Sandler, A.B., Miles, D., Coleman, R.L., Deurloo, R., and Chinot,
446 O.L. (2020). Bevacizumab (Avastin(R)) in cancer treatment: A review of 15 years of clinical
447 experience and future outlook. Cancer Treat Rev *86*, 102017. 10.1016/j.ctrv.2020.102017.
448 4. Detmar, M. (2000). Tumor angiogenesis. J Investig Dermatol Symp Proc *5*, 20-23.
449 10.1046/j.1087-0024.2000.00003.x.
450 5. Sato, Y., Yoshikawa, A., Yamagata, A., Mimura, H., Yamashita, M., Ookata, K., Nureki, O.,
451 Iwai, K., Komada, M., and Fukai, S. (2008). Structural basis for specific cleavage of Lys 63-
452 linked polyubiquitin chains. Nature *455*, 358-362. 10.1038/nature07254.
453 6. Chen, X., Shi, H., Bi, X., Li, Y., and Huang, Z. (2019). Targeting the deubiquitinase
454 STAMBPL1 triggers apoptosis in prostate cancer cells by promoting XIAP degradation.
455 Cancer Lett *456*, 49-58. 10.1016/j.canlet.2019.04.020.
456 7. Woo, S.M., Seo, S.U., Kubatka, P., Min, K.J., and Kwon, T.K. (2019). Honokiol Enhances
457 TRAIL-Mediated Apoptosis through STAMBPL1-Induced Survivin and c-FLIP
458 Degradation. Biomolecules *9*. 10.3390/biom9120838.
459 8. Liu, R., Yang, G., Bao, M., Zhou, Z., Mao, X., Liu, W., Jiang, X., Zhu, D., Ren, X., Huang, J.,
460 and Chen, C. (2022). STAMBPL1 promotes breast cancer cell resistance to cisplatin
461 partially by stabilizing MKP-1 expression. Oncogene *41*, 2265-2274. 10.1038/s41388-
462 022-02252-7.
463 9. Xing, Y.Q., Li, A., Yang, Y., Li, X.X., Zhang, L.N., and Guo, H.C. (2018). The regulation of
464 FOXO1 and its role in disease progression. Life Sci *193*, 124-131.
465 10.1016/j.lfs.2017.11.030.
466 10. Yu, J.M., Sun, W., Wang, Z.H., Liang, X., Hua, F., Li, K., Lv, X.X., Zhang, X.W., Liu, Y.Y., Yu,
467 J.J., et al. (2019). TRIB3 supports breast cancer stemness by suppressing FOXO1

468 degradation and enhancing SOX2 transcription. Nat Commun *10*, 5720.
469 10.1038/s41467-019-13700-6.
470 11. Cui, Q., Sun, J., Yuan, J., Li, J., Yang, C., Du, G., Zhou, C., Qiu, P., Gao, J., Zhang, Y., et al.
471 (2024). DNA damage chemotherapeutic drugs suppress basal-like breast cancer growth
472 by down-regulating the transcription of the FOXO1-KLF5 axis. Genes Dis *11*, 91-94.
473 10.1016/j.gendis.2023.03.028.
474 12. Jeon, H.H., Yu, Q., Lu, Y., Spencer, E., Lu, C., Milovanova, T., Yang, Y., Zhang, C.,
475 Stepanchenko, O., Vafa, R.P., et al. (2018). FOXO1 regulates VEGFA expression and
476 promotes angiogenesis in healing wounds. J Pathol *245*, 258-264. 10.1002/path.5075.
477 13. Chen, C., Sun, X., Ran, Q., Wilkinson, K.D., Murphy, T.J., Simons, J.W., and Dong, J.T.
478 (2005). Ubiquitin-proteasome degradation of KLF5 transcription factor in cancer and
479 untransformed epithelial cells. Oncogene *24*, 3319-3327. 10.1038/sj.onc.1208497.
480 14. Nagarajan, S., Bedi, U., Budida, A., Hamdan, F.H., Mishra, V.K., Najafova, Z., Xie, W., Alawi,
481 M., Indenbirken, D., Knapp, S., et al. (2017). BRD4 promotes p63 and GRHL3 expression
482 downstream of FOXO in mammary epithelial cells. Nucleic Acids Res *45*, 3130-3145.
483 10.1093/nar/gkw1276.
484 15. Ambroise, G., Yu, T.T., Zhang, B., Kacal, M., Hao, Y., Queiroz, A.L., Ouchida, A.T., Lindskog,
485 C., Norberg, E., and Vakifahmetoglu-Norberg, H. (2020). Systematic analysis reveals a
486 functional role for STAMBPL1 in the epithelial-mesenchymal transition process across
487 multiple carcinomas. *123*, 1164-1177. 10.1038/s41416-020-0972-x.
488 16. Liu, R., Yang, G., Bao, M., Zhou, Z., Mao, X., Liu, W., Jiang, X., Zhu, D., Ren, X., and Huang,
489 J. (2022). STAMBPL1 promotes breast cancer cell resistance to cisplatin partially by
490 stabilizing MKP-1 expression. *41*, 2265-2274. 10.1038/s41388-022-02252-7.
491 17. Wei, K., Ma, Z., Yang, F., Zhao, X., Jiang, W., Pan, C., Li, Z., Pan, X., He, Z., Xu, J., et al.
492 (2022). M2 macrophage-derived exosomes promote lung adenocarcinoma progression
493 by delivering miR-942. Cancer letters *526*, 205-216. 10.1016/j.canlet.2021.10.045.
494 18. Kim, S.Y., Ko, Y.S., Park, J., Choi, Y., Park, J.W., Kim, Y., Pyo, J.S., Yoo, Y.B., Lee, J.S., and
495 Lee, B.L. (2016). Forkhead Transcription Factor FOXO1 Inhibits Angiogenesis in Gastric
496 Cancer in Relation to SIRT1. Cancer research and treatment *48*, 345-354.
497 10.4143/crt.2014.247.
498 19. Dai, X., Xie, Y., and Dong, M. (2022). Cancer-associated fibroblasts derived extracellular
499 vesicles promote angiogenesis of colorectal adenocarcinoma cells through miR-135b-
500 5p/FOXO1 axis. *23*, 76-88. 10.1080/15384047.2021.2017222.
501 20. Shang, A., Wang, X., Gu, C., Liu, W., Sun, J., Zeng, B., Chen, C., Ji, P., Wu, J., Quan, W., et
502 al. (2020). Exosomal miR-183-5p promotes angiogenesis in colorectal cancer by
503 regulation of FOXO1. Aging *12*, 8352-8371. 10.18632/aging.103145.
504 21. Liu, Z., Du, D., and Zhang, S. (2024). Tumor-derived exosomal miR-1247-3p promotes
505 angiogenesis in bladder cancer by targeting FOXO1. *25*, 2290033.
506 10.1080/15384047.2023.2290033.
507 22. Darido, C., and Jane, S.M. (2010). Grhl3 and GEF19 in the front rho. Small GTPases *1*,
508 104-107. 10.4161/sgtp.1.2.13620.
509 23. Darido, C., Georgy, S.R., Wilanowski, T., Dworkin, S., Auden, A., Zhao, Q., Rank, G.,
510 Srivastava, S., Finlay, M.J., Papenfuss, A.T., et al. (2011). Targeting of the tumor
511 suppressor GRHL3 by a miR-21-dependent proto-oncogenic network results in PTEN

512 loss and tumorigenesis. Cancer cell *20*, 635-648. 10.1016/j.ccr.2011.10.014.
513 24. Guardiola-Serrano, F., Haendeler, J., Lukosz, M., Sturm, K., Melchner, H., and Altschmied,
514 J. (2008). Gene trapping identifies a putative tumor suppressor and a new inducer of cell
515 migration. Biochemical and biophysical research communications *376*, 748-752.
516 10.1016/j.bbrc.2008.09.070.
517 25. Fukuda, R., Hirota, K., Fan, F., Jung, Y.D., Ellis, L.M., and Semenza, G.L. (2002). Insulin-like
518 growth factor 1 induces hypoxia-inducible factor 1-mediated vascular endothelial
519 growth factor expression, which is dependent on MAP kinase and phosphatidylinositol
520 3-kinase signaling in colon cancer cells. The Journal of biological chemistry *277*, 38205-
521 38211. 10.1074/jbc.M203781200.
522 26. Zhong, H., Chiles, K., Feldser, D., Laughner, E., Hanrahan, C., Georgescu, M.M., Simons,
523 J.W., and Semenza, G.L. (2000). Modulation of hypoxia-inducible factor 1alpha
524 expression by the epidermal growth factor/phosphatidylinositol 3-
525 kinase/PTEN/AKT/FRAP pathway in human prostate cancer cells: implications for tumor
526 angiogenesis and therapeutics. Cancer research *60*, 1541-1545.
527 27. Hellwig-Bürgel, T., Stiehl, D.P., Wagner, A.E., Metzen, E., and Jelkmann, W. (2005).
528 Review: hypoxia-inducible factor-1 (HIF-1): a novel transcription factor in immune
529 reactions. Journal of interferon & cytokine research : the official journal of the
530 International Society for Interferon and Cytokine Research *25*, 297-310.
531 10.1089/jir.2005.25.297.
532 28. Kasuno, K., Takabuchi, S., Fukuda, K., Kizaka-Kondoh, S., Yodoi, J., Adachi, T., Semenza,
533 G.L., and Hirota, K. (2004). Nitric oxide induces hypoxia-inducible factor 1 activation that
534 is dependent on MAPK and phosphatidylinositol 3-kinase signaling. The Journal of
535 biological chemistry *279*, 2550-2558. 10.1074/jbc.M308197200.
536 29. Li, J., Davidson, G., Huang, Y., Jiang, B.H., Shi, X., Costa, M., and Huang, C. (2004). Nickel
537 compounds act through phosphatidylinositol-3-kinase/Akt-dependent, p70(S6k)-
538 independent pathway to induce hypoxia inducible factor transactivation and Cap43
539 expression in mouse epidermal Cl41 cells. Cancer research *64*, 94-101. 10.1158/0008-
540 5472.can-03-0737.
541 30. Mazure, N.M., Chen, E.Y., Laderoute, K.R., and Giaccia, A.J. (1997). Induction of vascular
542 endothelial growth factor by hypoxia is modulated by a phosphatidylinositol 3-
543 kinase/Akt signaling pathway in Ha-ras-transformed cells through a hypoxia inducible
544 factor-1 transcriptional element. Blood *90*, 3322-3331.
545 31. Pore, N., Jiang, Z., Shu, H.K., Bernhard, E., Kao, G.D., and Maity, A. (2006). Akt1 activation
546 can augment hypoxia-inducible factor-1alpha expression by increasing protein
547 translation through a mammalian target of rapamycin-independent pathway. Molecular
548 cancer research : MCR *4*, 471-479. 10.1158/1541-7786.mcr-05-0234.

549

550 **Figures and legends**

551 **Figure 1. STAMBPL1 upregulates HIF1α in a non-enzymatic manner in TNBC cells. (A)**
552 After STAMBPL1 was knocked down in HCC1806 and HCC1937 cells and then subjected to
553 hypoxia for 10 h, STAMBPL1 knockdown downregulated the protein level of HIF1α. **(B-C)**
554 RNA samples were collected after 10 h of hypoxia treatment following the knockdown of
555 STAMBPL1 in HCC1806 cells. RT–qPCR experiments revealed that the knockdown of
556 STAMBPL1 downregulated the mRNA levels of the HIF1α downstream targets *VEGFA* and
557 *GLUT1*. **(D-E)** RNA samples were collected after 10 hours of hypoxia treatment following the
558 knockdown of STAMBPL1 in HCC1937 cells. RT–qPCR experiments revealed that the
559 knockdown of STAMBPL1 downregulated the mRNA levels of the HIF1α downstream targets
560 *VEGFA* and *GLUT1*. **(F)** Overexpression of STAMBPL1/STAMBPL1-E292A upregulated
561 HIF1α protein expression in HCC1806 and HCC1937 cells stably overexpressing
562 STAMBPL1/STAMBPL1-E292A under normoxia. *: $P<0.05$, **: $P<0.01$, ***: $P<0.001$, *t* test.

563 **Figure 2. STAMBPL1 promotes *HIF1A* transcription and activates the HIF1α/VEGFA**
564 **axis. (A)** Western blot analysis was performed to confirm the knockdown of STAMBPL1 in
565 HCC1806 and HCC1937 cells. **(B)** RNA samples were collected after 10 h of hypoxia
566 treatment following the knockdown of STAMBPL1 in HCC1806 cells. RT–qPCR experiments
567 revealed that the knockdown of STAMBPL1 could downregulate the mRNA levels of HIF1α.
568 **(C)** RNA samples were collected after 10 hours of hypoxia treatment following the knockdown
569 of STAMBPL1 in HCC1937 cells. RT–qPCR experiments revealed that the knockdown of
570 STAMBPL1 downregulated the mRNA levels of HIF1α. **(D)** HCC1806 cells stably
571 overexpressing STAMBPL1 were used to knock down HIF1α via siRNA. The protein was then

572 collected and subjected to Western blotting experiments. The results showed that the
573 overexpression of STAMBPL1 promoted the expression of HIF1α, which could be rescued by
574 the knockdown of HIF1α. **(E)** HIF1α was knocked down in HCC1806 cells stably
575 overexpressing STAMBPL1 via siRNA. The RNA was then collected and subjected to RT–
576 qPCR experiments. The results showed that the overexpression of STAMBPL1 promoted the
577 expression of the VEGFA mRNA, which could be rescued by the knockdown of HIF1α. **(F)** In
578 HCC1937 cells stably overexpressing STAMBPL1, HIF1α was knocked down via siRNA, and
579 protein was collected. Western blotting experiments revealed that the overexpression of
580 STAMBPL1 promoted HIF1α expression, which could be rescued by the knockdown of HIF1α.
581 **(G)** In HCC1937 cells stably overexpressing STAMBPL1, HIF1α was knocked down via
582 siRNA, and RNA was collected. RT–qPCR experiments revealed that the overexpression of
583 STAMBPL1 promoted VEGFA mRNA expression, which could be rescued by the knockdown
584 of HIF1α. *: $P<0.05$, **: $P<0.01$, ***: $P<0.001$, *t* test.

585 **Figure 3. STAMBPL1 in TNBC cells enhances the activity of HUVECs and promotes**
586 **TNBC angiogenesis. (A)** In HCC1806 cells, STAMBPL1 was knocked down via siRNA, and
587 the cells were then subjected to hypoxia for 24 hours. The conditioned medium (CM)
588 collected from these cells was used to treat HUVECs. EdU assays revealed that the
589 conditioned medium after STAMBPL1 knockdown inhibited the proliferation of HUVECs. **(B)**
590 Statistical analysis of the EdU assay results. **(C)** In HCC1806 cells, STAMBPL1 was knocked
591 down via siRNA, and the cells were then subjected to hypoxia for 24 hours. The CM collected
592 from these cells was used to treat HUVECs. Wound healing assays demonstrated that the
593 conditioned medium after STAMBPL1 knockdown inhibited the migration of HUVECs. **(D)**

594 Statistical analysis of the wound healing assay results. **(E)** In HCC1806 cells, STAMBPL1 was
595 knocked down via siRNA, and the cells were then subjected to hypoxia for 24 hours. The CM
596 collected from these cells was used to treat HUVECs. A tube formation assay revealed that
597 the conditioned medium after STAMBPL1 knockdown inhibited the tube formation of
598 HUVECs. **(F)** Statistical analysis of the tube formation assay results. **(G)** The growth of TNBC
599 xenograft tumors was evaluated by photographing the tumors in nude mice to assess the role
600 of STAMBPL1. Knockdown of STAMBPL1 significantly inhibited tumor growth. **(H-I)** The
601 growth and weight of the transplanted tumors in the nude mice were statistically analyzed,
602 and the STAMBPL1sh#1 and STAMBPL1sh#2 groups were compared with the shLuc group.
603 **(J)** An immunohistochemical assay was used to detect the expression of the angiogenesis
604 marker CD31 in xenograft tumors. **(K)** The number of microvessels in the
605 immunohistochemical experiments was statistically analyzed. *: $P<0.05$, **: $P<0.01$, ***:
606 $P<0.001$, *t* test.

607 **Figure 4. STAMBPL1 promotes *HIF1A* transcription via the upregulation of GRHL3. (A)**
608 Venn diagram showing the overlap of differentially expressed genes identified via RNA-seq
609 analysis. **(B)** RT–qPCR experiments demonstrated that the knockdown of STAMBPL1
610 resulted in decreased mRNA levels of GRHL3 in HCC1806 cells. **(C)** In HCC1806 cells stably
611 overexpressing STAMBPL1, GRHL3 was knocked down via siRNA, after which the protein
612 was collected. Western blotting experiments revealed that the overexpression of STAMBPL1
613 promoted the expression of HIF1α, which could be rescued by the knockdown of GRHL3. **(D-**
614 **F)** In HCC1806 cells stably overexpressing STAMBPL1, GRHL3 was knocked down via
615 siRNA, and RNA was subsequently collected. RT–qPCR experiments revealed that the

616 overexpression of STAMBPL1 upregulated the mRNA expression of GRHL3, HIF1α and its
617 downstream target VEGFA, which could be rescued by the knockdown of GRHL3. **(G)**
618 Statistical analysis of the EdU assay results. **(H)** Statistical analysis of the wound healing
619 assay results. **(I)** Statistical analysis of the tube formation assay results. *: $P<0.05$, **: $P<0.01$,
620 ***: $P<0.001$, *t* test.

621 **Figure 5. GRHL3 enhances *HIF1A* transcription by binding to its promoter. (A)** The
622 JASPAR website was used to predict the potential binding sequence of the transcription factor
623 GRHL3 to the HIF1α promoter. **(B)** Mutation pattern of the HIF1α promoter binding sequence.
624 **(C)** Overexpression of GRHL3 in HCC1806 cells stably overexpressing GRHL3 resulted in
625 increased protein expression of HIF1α. **(D)** ChIP–PCR experiments conducted in HCC1806
626 cells stably overexpressing GRHL3 revealed that GRHL3 could bind to the promoter region of
627 the target gene *HIF1A*. **(E)** A luciferase assay performed in HEK293T cells indicated that
628 GRHL3 could bind to the promoter sequence of *HIF1A* and increase its transcriptional activity.
629 **(F)** In HCC1806 cells, GRHL3 was knocked down by siRNA, and the cells were subjected to
630 hypoxia for 4 hours. Western blotting experiments revealed that the knockdown of GRHL3
631 downregulated the protein level of HIF1α. **(G-I)** In HCC1806 cells, GRHL3 was knocked down
632 by siRNA, followed by hypoxia treatment for 4 hours, after which RNA samples were
633 collected. RT–qPCR experiments revealed that GRHL3 knockdown was effective and that the
634 knockdown of GRHL3 could downregulate the mRNA levels of HIF1α and its downstream
635 target VEGFA. **(J)** In HCC1806 cells, GRHL3 was knocked down via siRNA, and the cells
636 were then subjected to hypoxia for 24 hours. The conditioned medium was collected and
637 used to treat HUVECs. EdU assays revealed that the conditioned medium after GRHL3

638 knockdown inhibited the proliferation of HUVECs. Statistical analysis of the EdU assay results
639 was performed. **(K)** In HCC1806 cells, GRHL3 was knocked down via siRNA, and the cells
640 were then subjected to hypoxia for 24 hours. The conditioned medium was collected and
641 used to treat HUVECs. Wound healing assays revealed that the conditioned medium after
642 GRHL3 knockdown inhibited the migration of HUVECs. Statistical analysis of the wound
643 healing assay results was performed. **(L)** In HCC1806 cells, GRHL3 was knocked down via
644 siRNA, and the cells were then subjected to hypoxia for 24 hours. The conditioned medium
645 was collected and used to treat HUVECs. The results of the tube formation assay revealed
646 that conditioned medium from GRHL3-knockdown HUVECs inhibited tube formation.
647 Statistical analysis of the tube formation assay results was performed. *: $P<0.05$, **: $P<0.01$,
648 ***: $P<0.001$, *t* test.

649 **Figure 6. GRHL3 enhances *HIF1A* transcription by binding to its promoter. (A)** In
650 HCC1806 cells stably overexpressing GRHL3, HIF1α was knocked down by siRNA, and the
651 protein was subsequently collected. Western blotting experiments revealed that the
652 overexpression of GRHL3 promoted the expression of HIF1α, which could be rescued by the
653 knockdown of HIF1α. **(B)** In HCC1806 cells stably overexpressing GRHL3, HIF1α was
654 knocked down by siRNA, and then the RNA was collected. RT–qPCR experiments revealed
655 that the overexpression of GRHL3 promoted the expression of the VEGFA mRNA, which
656 could be rescued by the knockdown of HIF1α. **(C)** HCC1806 cells stably overexpressing
657 GRHL3 were used for the knockdown of HIF1α via siRNA. The conditioned medium was then
658 collected and used to treat HUVECs. EdU assays revealed that the overexpression of GRHL3
659 promoted the proliferation of HUVECs, which could be rescued by the knockdown of HIF1α.

660 **(D)** HCC1806 cells stably overexpressing GRHL3 were used for the knockdown of HIF1α via
661 siRNA. The conditioned medium was then collected and used to treat HUVECs. A wound
662 healing assay revealed that the overexpression of GRHL3 promoted the migration of
663 HUVECs, which could be rescued by the knockdown of HIF1α. **(E)** HCC1806 cells stably
664 overexpressing GRHL3 were used for the knockdown of HIF1α via siRNA. The conditioned
665 medium was then collected and used to treat HUVECs. The tube formation assay revealed
666 that the overexpression of GRHL3 promoted the tube formation of HUVECs, which could be
667 rescued by the knockdown of HIF1α. **(F)** RT–qPCR was used to detect the knockdown of
668 GRHL3 in HCC1806 cells. **(G)** Photographs of xenograft tumors from nude mice were taken
669 to evaluate the role of GRHL3 in the growth of TNBC xenograft tumors. The results showed
670 that the knockdown of GRHL3 significantly inhibited tumor growth. **(H)** The weights of the
671 transplanted tumors from the nude mice were statistically analyzed, and the shGRHL3 1# and
672 shGRHL3 2# groups were compared with the shLuc group. **(I)** The growth of transplanted
673 tumors in nude mice was statistically analyzed, and the shGRHL3 1# and shGRHL3 2#
674 groups were compared with the shLuc group. **(J)** An immunohistochemical assay was
675 performed to detect the expression of the angiogenesis marker CD31 in xenograft tumors. **(K)**
676 Statistical analysis of the number of microvessels in the immunohistochemical experiments. *:
677 $P<0.05$, **: $P<0.01$, ***: $P<0.001$, *t* test.

678 **Figure 7. STAMBPL1 mediates *GRHL3* transcription by interacting with FOXO1. (A)**
679 Western blotting experiments revealed that the knockdown of FOXO1 in HCC1806 cells
680 followed by hypoxia treatment for 4 hours inhibited HIF1α protein expression. **(B-D)** RT–
681 qPCR experiments revealed that the knockdown of FOXO1 in HCC1806 cells followed by

682 hypoxia treatment for 4 hours decreased the mRNA levels of GRHL3/HIF1α/VEGFA. **(E)** In
683 HCC1806 cells stably overexpressing STAMBPL1, protein samples were collected after
684 FOXO1 was knocked down via siRNA. Western blotting experiments revealed that the
685 overexpression of STAMBPL1 promoted the expression of HIF1α, which could be rescued by
686 the knockdown of FOXO1. **(F-H)** In HCC1806 cells stably overexpressing STAMBPL1, RNA
687 samples were collected after the knockdown of FOXO1 via siRNA. RT–qPCR experiments
688 revealed that the overexpression of STAMBPL1 promoted the mRNA expression of GRHL3,
689 HIF1α and VEGFA, which could be rescued by the knockdown of FOXO1. **(I)** An endogenous
690 ChIP–PCR assay was performed using an anti-FOXO1 antibody in HCC1806 cells. **(J)** A
691 luciferase assay performed in HEK293T cells revealed that FOXO1 was able to bind to the
692 promoter sequence of GRHL3 and increase its transcriptional activity. **(K)** A luciferase assay
693 conducted in HEK293T cells revealed that STAMBPL1 enhanced the activation of the GRHL3
694 promoter by FOXO1. **(L)** ChIP–PCR experiments were performed in HCC1806 cells stably
695 overexpressing STAMBPL1 after knocking down FOXO1 via siRNA. **(M)** PCDH-STAMBPL1-
696 3×Flag and PCDH-FOXO1-3×Flag plasmids were cotransfected into HEK293T cells, and
697 then, immunofluorescence experiments were performed. Red represents STAMBPL1
698 staining, green represents FOXO1 staining, and blue represents DAPI staining. **(N)**
699 Endogenous STAMBPL1 protein was immunoprecipitated from HCC1937 cells via an anti-
700 FOXO1 antibody. Immunoglobulin G (IgG) served as the negative control. Endogenous
701 STAMBPL1 was detected via western blotting. *: $P<0.05$, **: $P<0.01$, ***: $P<0.001$, *t* test.

702 **Figure 8. The combination of VEGFR and FOXO1 inhibitors synergistically suppresses**
703 **TNBC xenograft growth. (A-C)** TCGA database analysis revealed high expression levels of

704 STAMBPL1, FOXO1, and GRHL3 in TNBC. **(D)** The effect of STAMBPL1 overexpression in
705 HCC1806 cells was detected by Western blotting. **(E)** The effect of drug treatment on
706 transplanted tumors in nude mice was evaluated by photographing the tumors. The
707 overexpression of STAMBPL1 promoted tumor growth, whereas the combination of the
708 FOXO1 inhibitor AS1842856 (10 mg/kg, every two days) and the VEGFR inhibitor apatinib (50
709 mg/kg, every two days) significantly inhibited tumor growth. **(F-G)** The weight and growth of
710 the transplanted tumors in the nude mice were statistically analyzed. The vector control group
711 and the STAMBPL overexpression group were compared. The nondrug group and the
712 combined drug group in the vector control group were compared. The nondrug group and the
713 combined drug group in the STAMBPL overexpression group were compared. **(H)** The final
714 weights of the nude mice were statistically analyzed. *: $P<0.05$, **: $P<0.01$, ***: $P<0.001$, *t*
715 test.

716 **Figure 9. The working model of this study.** STAMBPL1 interacts with FOXO1 to promote
717 TNBC angiogenesis by activating the GRHL3/HIF1α/VEGFA axis.

718 **Additional material**

719 **Supplementary Material 1**

720 **Figure S1. STAMBPL1 in TNBC cells enhances the activity of HUVECs. (A)** HCC1937
721 cells were transfected with STAMBPL1 siRNA and subjected to hypoxia for 24 hours. The
722 conditioned medium collected from these cells was then used to treat HUVECs. EdU assay
723 revealed that the conditioned medium after STAMBPL1 knockdown inhibited the proliferation
724 of HUVECs. **(B)** Statistical analysis of the EdU assay results. **(C)** HCC1937 cells were
725 transfected with STAMBPL1 siRNA and subjected to hypoxia for 24 hours. The conditioned

726 medium collected from these cells was used to treat HUVECs. Wound healing assay
727 demonstrated that the conditioned medium after STAMBPL1 knockdown inhibited the
728 migration of HUVECs. **(D)** Statistical analysis of the wound healing assay results. **(E)**
729 HCC1937 cells were transfected with STAMBPL1 siRNA and subjected to hypoxia for 24
730 hours. The conditioned medium collected from these cells was used to treat HUVECs. Tube
731 formation assay showed that the conditioned medium after STAMBPL1 knockdown inhibited
732 tube formation of HUVECs. **(F)** Statistical analysis of the tube formation assay results. *:
733 $P<0.05$, **: $P<0.01$, ***: $P<0.001$, *t* test.

734 **Figure S2. STAMBPL1 in TNBC cells enhances the activity of HUVECs. (A and D)**
735 HCC1806 and HCC1937 cells were stably overexpressing STAMBPL1, and HIF1α was
736 knocked down using siRNA. The conditioned medium was then collected and used to treat
737 HUVECs. EdU assay results demonstrated that the overexpression of STAMBPL1 promoted
738 the proliferation of HUVECs, which could be rescued by knockdown of HIF1α. Statistical
739 analysis of the EdU assay results was performed. **(B and E)** HCC1806 and HCC1937 cells
740 stably overexpressing STAMBPL1 were used to knock down HIF1α using siRNA. The
741 conditioned medium was collected and used to treat HUVECs. Wound healing assay results
742 showed that the overexpression of STAMBPL1 promoted the migration of HUVECs, which
743 could be rescued by knockdown of HIF1α. Statistical analysis of the wound healing assay
744 results was performed. **(C and F)** HCC1806 and HCC1937 cells stably overexpressing
745 STAMBPL1 were used to knock down HIF1α using siRNA. The conditioned medium was
746 collected and used to treat HUVECs. Tube formation assay results showed that the
747 overexpression of STAMBPL1 promoted the tube formation of HUVECs, which could be

748 rescued by knockdown of HIF1α. Statistical analysis of the tube formation assay results was
749 performed. *: $P<0.05$, **: $P<0.01$, ***: $P<0.001$, *t* test.

750 **Figure S3. STAMBPL1 promotes *HIF1A* transcription via upregulating GRHL3. (A)** RNA-
751 seq result: the list of 18 genes downregulated after STAMBPL1 knockdown in HCC1806 cells.
752 **(B)** RT-qPCR experiments showed that knockdown of STAMBPL1 inhibited GRHL3 mRNA
753 levels in HCC1937 cells. **(C)** In HCC1937 cells stably overexpressing STAMBPL1, GRHL3
754 was knocked down using siRNA, and then the protein was collected. Western blotting
755 experiments showed that overexpression of STAMBPL1 promoted the expression of HIF1α,
756 which could be rescued by knockdown of GRHL3. **(D-F)** In HCC1937 cells stably
757 overexpressing STAMBPL1, GRHL3 was knocked down using siRNA and then the RNA was
758 collected. RT-qPCR experiments showed that overexpression of STAMBPL1 promoted the
759 mRNA expression of GRHL3, HIF1α and its downstream target VEGFA, which could be
760 rescued by knockdown of GRHL3. **(G)** Statistical analysis of EdU assay. **(H)** Statistical
761 analysis of wound healing assay. **(I)** Statistical analysis of tube formation assay. *: $P<0.05$, **:
762 $P<0.01$, ***: $P<0.001$, *t* test.

763 **Figure S4. GRHL3 enhances *HIF1A* transcription by binding to its promoter. (A)** In
764 HCC1937 cells, knockdown of GRHL3 using siRNA and treated with hypoxia for 4 hours.
765 Western blotting experiments showed that knockdown of GRHL3 could down-regulate the
766 protein level of HIF1α. **(B-D)** In HCC1937 cells, GRHL3 was knocked down by siRNA,
767 followed by hypoxia treatment for 4 hours, and then RNA samples were collected. RT-qPCR
768 experiments showed that GRHL3 knockdown was effective, and knockdown of GRHL3 could
769 down-regulate the mRNA levels of HIF1α and its downstream target VEGFA. **(E)** In HCC1937

770 cells, GRHL3 was knocked down by siRNA and then treated with hypoxia for 24 hours, and
771 then the conditioned medium was collected to treat HUVECs, EdU assay showed that the
772 conditioned medium after knocking down GRHL3 inhibited the proliferation of HUVECs. **(F)** In
773 HCC1937 cells, GRHL3 was knocked down by siRNA and then treated with hypoxia for 24
774 hours, and then the conditioned medium was collected to treat HUVECs, wound healing
775 assay showed that the conditioned medium after knocking down GRHL3 inhibited the
776 migration of HUVECs. **(G)** In HCC1937 cells, GRHL3 was knocked down by siRNA and then
777 treated with hypoxia for 24 hours, and then the conditioned medium was collected to treat
778 HUVECs, the tube formation assay showed that the conditioned medium after knocking down
779 GRHL3 inhibited tube formation of HUVECs. **(H)** In HCC1937 cells stably overexpressing
780 GRHL3, HIF1α was knocked down using siRNA, and then the protein was collected. Western
781 blotting experiments showed that overexpression of GRHL3 promoted the expression of
782 HIF1α, which could be rescued by knockdown of HIF1α. **(I)** In HCC1937 cells stably
783 overexpressing GRHL3, HIF1α was knocked down using siRNA and then the RNA was
784 collected. RT-qPCR experiments showed that overexpression of GRHL3 promoted the mRNA
785 expression of VEGFA, which could be rescued by knockdown of HIF1α. **(J)** Statistical
786 analysis of EdU assay results. **(K)** Statistical analysis of wound healing assay results. **(L)**
787 Statistical analysis of tube formation assay results. *: $P<0.05$, **: $P<0.01$, ***: $P<0.001$, *t* test.
788 **Figure S5. STAMBPL1 mediates *GRHL3* transcription by interacting with FOXO1. (A)**
789 Western blotting experiments showed that knockdown of FOXO1 in HCC1937 cells followed
790 by hypoxia treatment for 4 hours inhibited HIF1α protein expression. **(B-D)** RT-qPCR
791 experiments showed that knockdown of FOXO1 in HCC1937 cells followed by hypoxia

792 treatment for 4 hours inhibited the mRNA levels of GRHL3/HIF1α/VEGFA. **(E)** The JASPAR
793 website predicts the possible binding sequence of transcription factor FOXO1 to the GRHL3
794 promoter and its mutation pattern map. **(F)** The truncated structure diagram of STAMBPL1.
795 **(G)** The truncated structure diagram of FOXO1. **(H)** The full-length and truncated plasmids of
796 pEBG-STAMBPL1-GST and pCDH-FOXO1-no tag were transfected into HEK293T cells, and
797 the proteins were collected for GST-pull down assay at 48 hours after transfection. **(I)** The full-
798 length and truncated plasmids of pCDH-FOXO1-3×Flag and pEBG-STAMBPL1-GST were
799 transfected into HEK293T cells, and the proteins were collected for IP-Flag assay at 48 hours
800 after transfection. *: $P<0.05$, **: $P<0.01$, ***: $P<0.001$, *t* test.

Figure 1

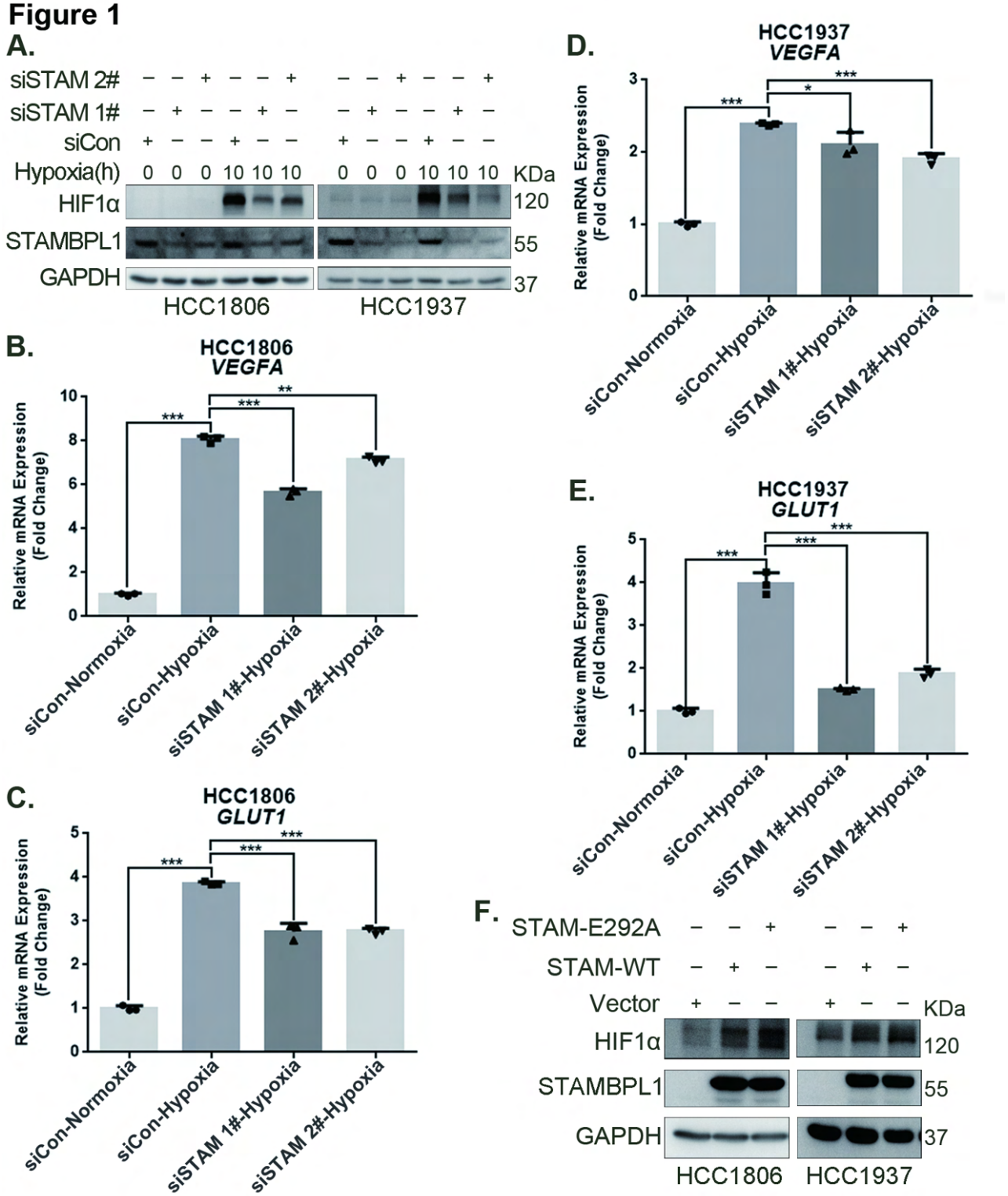
A.
siSTAM 2# − − + − − + − − + − − +
siSTAM 1# − + − − + − − + − − + −
siCon + − − + − − + − − + − −
Hypoxia(h) 0 0 0 10 10 10 0 0 0 10 10 10
KDa
HIF1α
120
STAMBPL1
55
GAPDH
37
HCC1806
HCC1937
B.
HCC1806
VEGFA
Relative mRNA Expression (Fold Change)
siCon-Normoxia
siCon-Hypoxia
siSTAM 1#-Hypoxia
siSTAM 2#-Hypoxia
C.
HCC1806
GLUT1
D.
HCC1937
VEGFA
E.
HCC1937
GLUT1
F.
STAM-E292A − − + − − +
STAM-WT − + − − + −
Vector + − − + − −
KDa
HIF1α
120
STAMBPL1
55
GAPDH
37
HCC1806
HCC1937

Figure 2

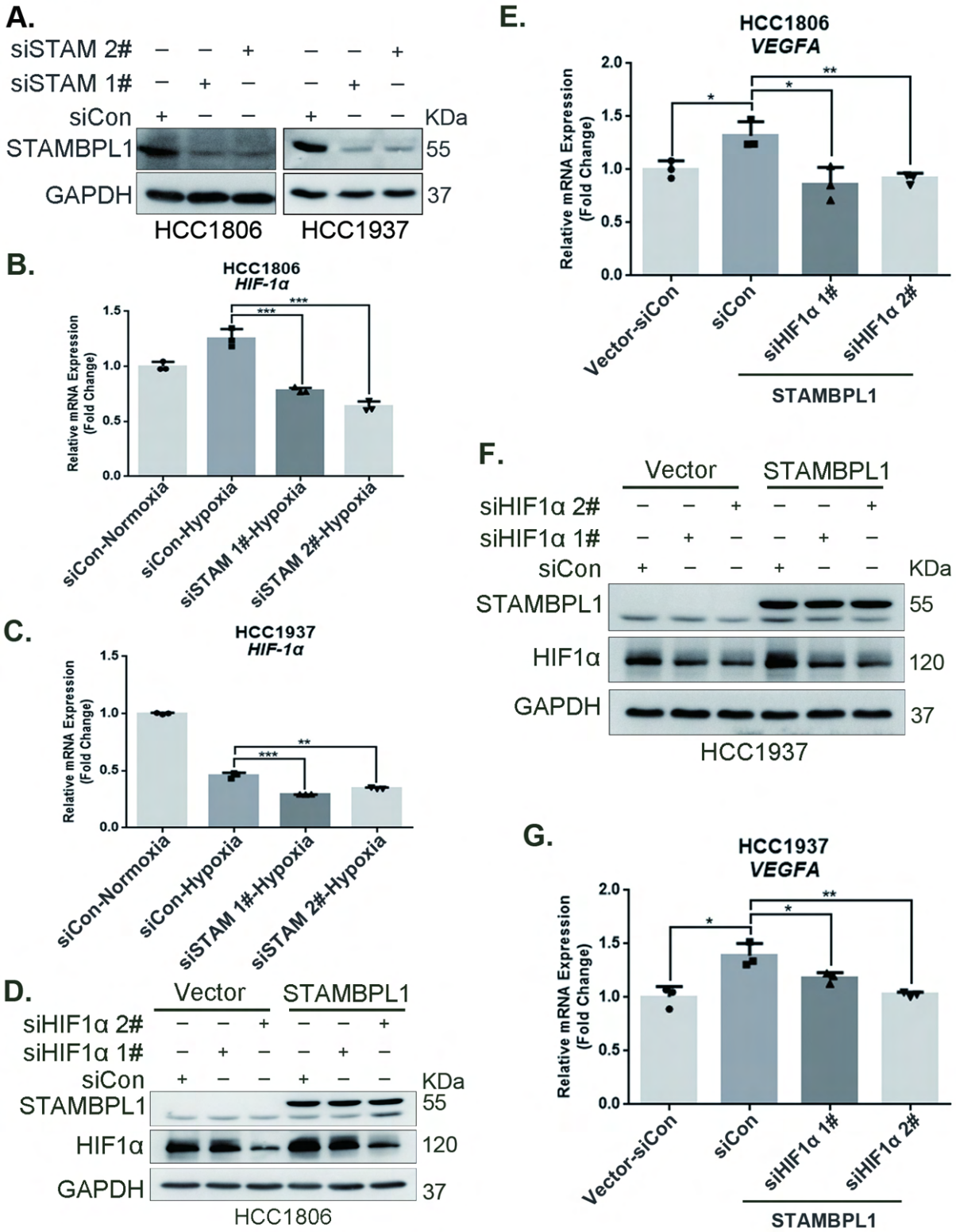
A.
siSTAM 2#
siSTAM 1#
siCon
STAMBPL1
GAPDH
KDa
55
37
HCC1806
HCC1937
B.
HCC1806
HIF-1α
Relative mRNA Expression (Fold Change)
siCon-Normoxia
siCon-Hypoxia
siSTAM 1#-Hypoxia
siSTAM 2#-Hypoxia
C.
HCC1937
HIF-1α
D.
Vector
STAMBPL1
siHIF1α 2#
siHIF1α 1#
siCon
HIF1α
120
HCC1806
E.
HCC1806
VEGFA
Vector-siCon
siCon
siHIF1α 1#
siHIF1α 2#
F.
HCC1937
G.
HCC1937
VEGFA

Figure 3

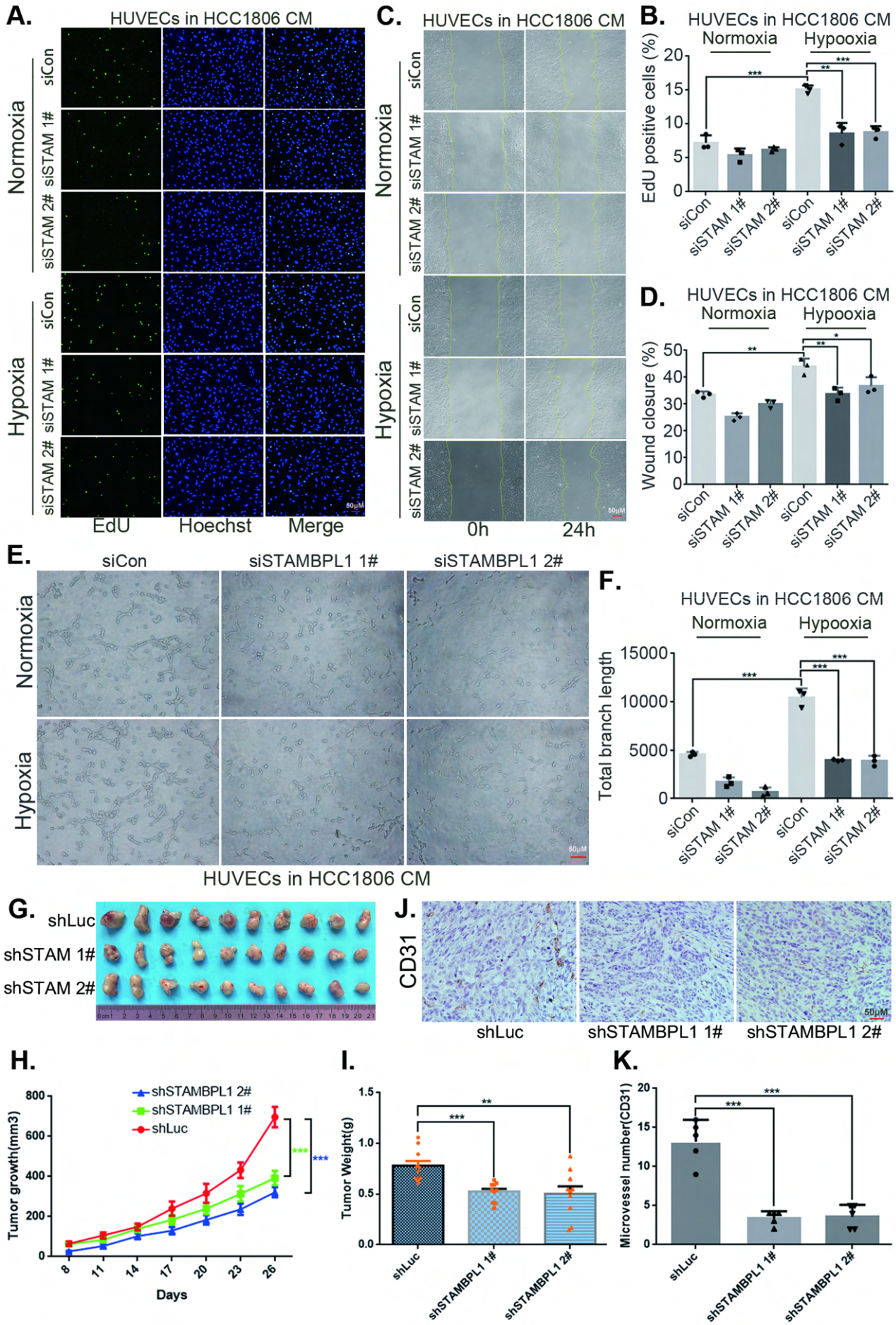
A.
HUVECs in HCC1806 CM
Normoxia
Hypoxia
siCon
siSTAM 1#
siSTAM 2#
EdU
Hoechst
Merge
C.
HUVECs in HCC1806 CM
0h
24h
B.
HUVECs in HCC1806 CM
Normoxia
Hypooxia
EdU positive cells (%)
D.
HUVECs in HCC1806 CM
Wound closure (%)
E.
siCon
siSTAMBPL1 1#
siSTAMBPL1 2#
F.
HUVECs in HCC1806 CM
Total branch length
G.
shLuc
shSTAM 1#
shSTAM 2#
J.
CD31
shLuc
shSTAMBPL1 1#
shSTAMBPL1 2#
H.
shSTAMBPL1 2#
shSTAMBPL1 1#
shLuc
Tumor growth(mm3)
Days
I.
Tumor Weight(g)
K.
Microvessel number(CD31)

Figure 4

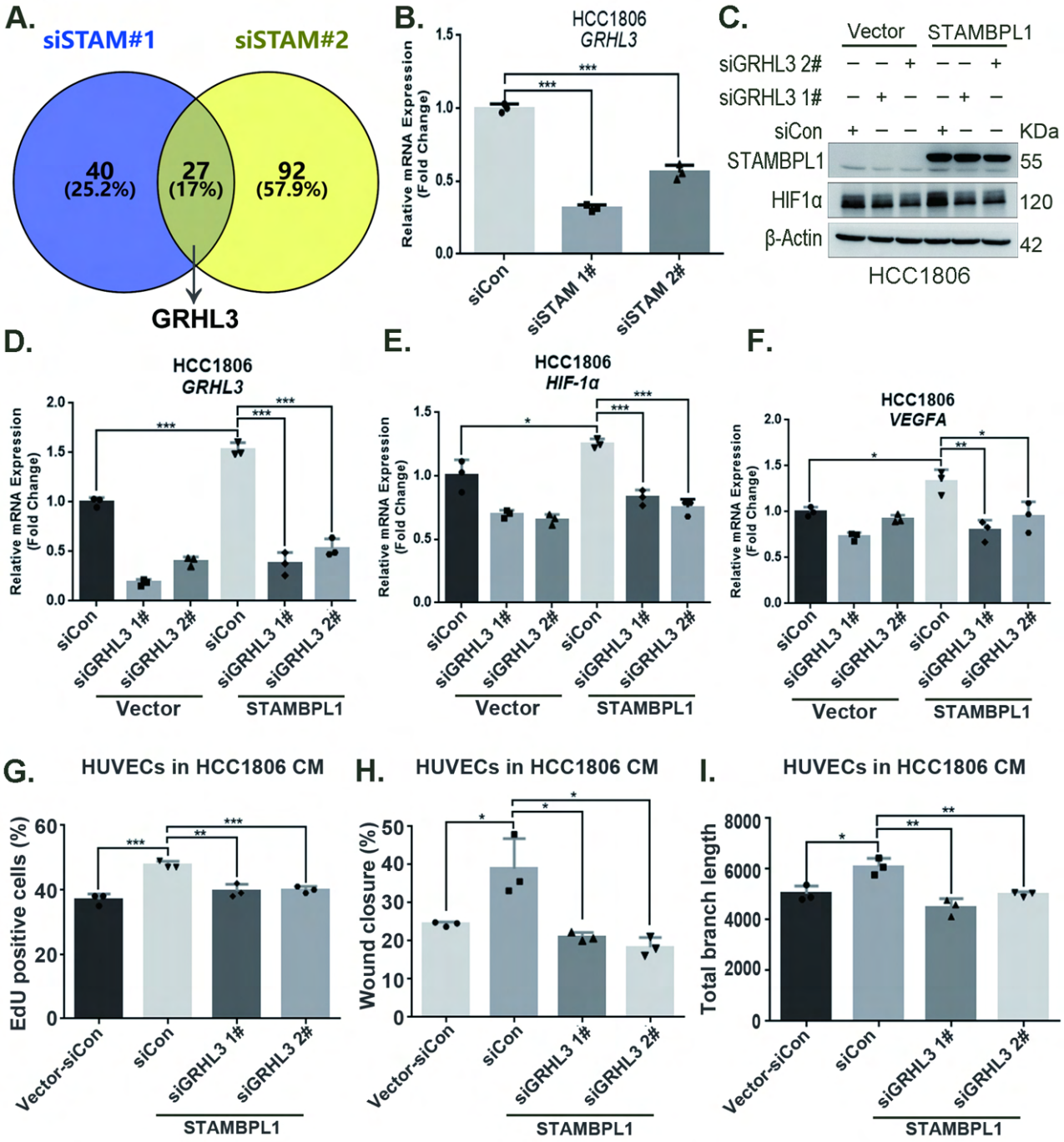
A.
siSTAM#1
siSTAM#2
40 (25.2%)
27 (17%)
92 (57.9%)
GRHL3
B.
HCC1806
GRHL3
Relative mRNA Expression (Fold Change)
siCon
siSTAM 1#
siSTAM 2#
C.
Vector
STAMBPL1
siGRHL3 2#
siGRHL3 1#
siCon
KDa
STAMBPL1
HIF1α
β-Actin
55
120
42
HCC1806
D.
HCC1806
GRHL3
E.
HCC1806
HIF-1α
F.
HCC1806
VEGFA
siGRHL3 1#
siGRHL3 2#
Vector
STAMBPL1
G.
HUVECs in HCC1806 CM
EdU positive cells (%)
H.
HUVECs in HCC1806 CM
Wound closure (%)
I.
HUVECs in HCC1806 CM
Total branch length
Vector-siCon

Figure 5

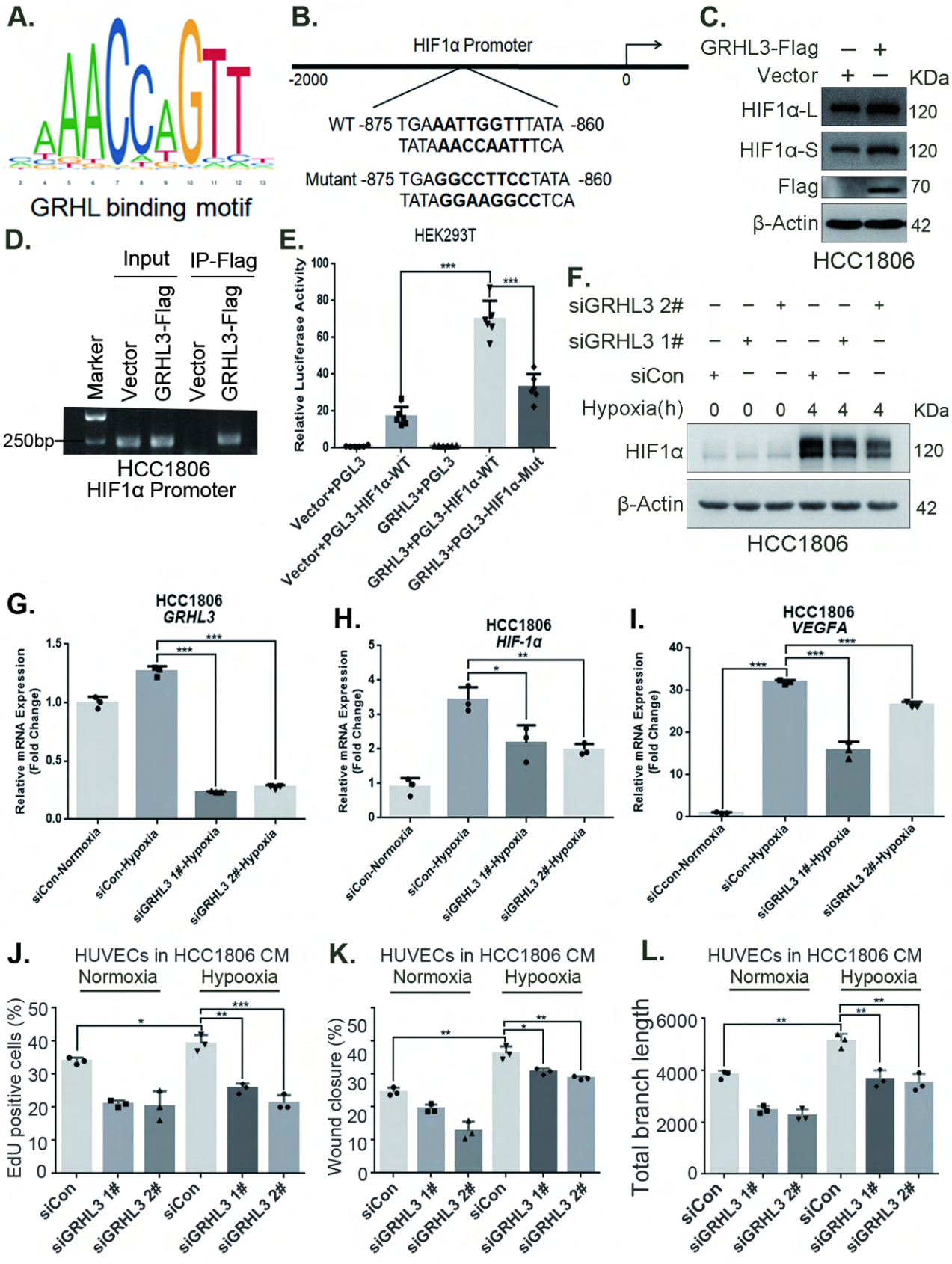
A.
GRHL binding motif
B.
HIF1α Promoter
-2000
0
WT -875 TGAAATTGGTTTATA -860
TATAAACCAATTTCA
Mutant -875 TGAGGCCTTCCTATA -860
TATAGGAAGGCCTCA
C.
GRHL3-Flag
Vector
KDa
HIF1α-L
HIF1α-S
Flag
β-Actin
120
120
70
42
HCC1806
D.
Input
IP-Flag
Marker
Vector
GRHL3-Flag
Vector
GRHL3-Flag
250bp
HCC1806
HIF1α Promoter
E.
HEK293T
Relative Luciferase Activity
Vector+PGL3
Vector+PGL3-HIF1α-WT
GRHL3+PGL3
GRHL3+PGL3-HIF1α-WT
GRHL3+PGL3-HIF1α-Mut
F.
siGRHL3 2#
siGRHL3 1#
siCon
Hypoxia(h)
0 0 0 4 4 4
KDa
HIF1α
β-Actin
120
42
HCC1806
G.
HCC1806
GRHL3
Relative mRNA Expression (Fold Change)
siCon-Normoxia
siCon-Hypoxia
siGRHL3 1#-Hypoxia
siGRHL3 2#-Hypoxia
H.
HCC1806
HIF-1α
I.
HCC1806
VEGFA
J.
HUVECs in HCC1806 CM
Normoxia
Hypooxia
EdU positive cells (%)
siCon
siGRHL3 1#
siGRHL3 2#
K.
Wound closure (%)
L.
Total branch length

Figure 6

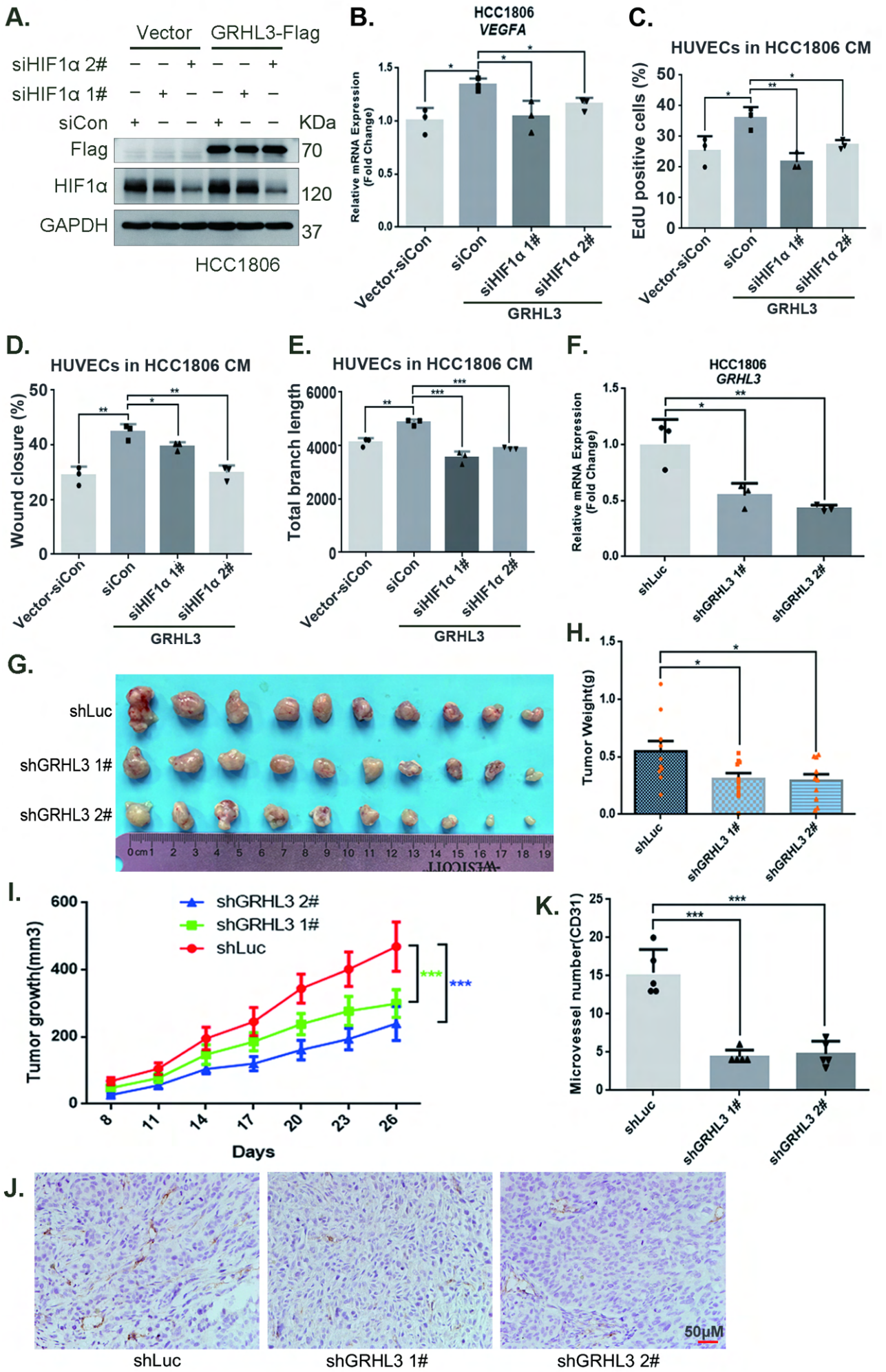
A.
Vector
GRHL3-Flag
siHIF1α 2#
siHIF1α 1#
siCon
KDa
Flag
HIF1α
GAPDH
70
120
37
HCC1806
B.
HCC1806
VEGFA
Relative mRNA Expression (Fold Change)
Vector-siCon
siCon
siHIF1α 1#
siHIF1α 2#
GRHL3
C.
HUVECs in HCC1806 CM
EdU positive cells (%)
D.
HUVECs in HCC1806 CM
Wound closure (%)
E.
HUVECs in HCC1806 CM
Total branch length
F.
HCC1806
GRHL3
shLuc
shGRHL3 1#
shGRHL3 2#
G.
H.
Tumor Weight(g)
I.
Tumor growth(mm3)
Days
K.
Microvessel number(CD31)
J.
50μM

Figure 7

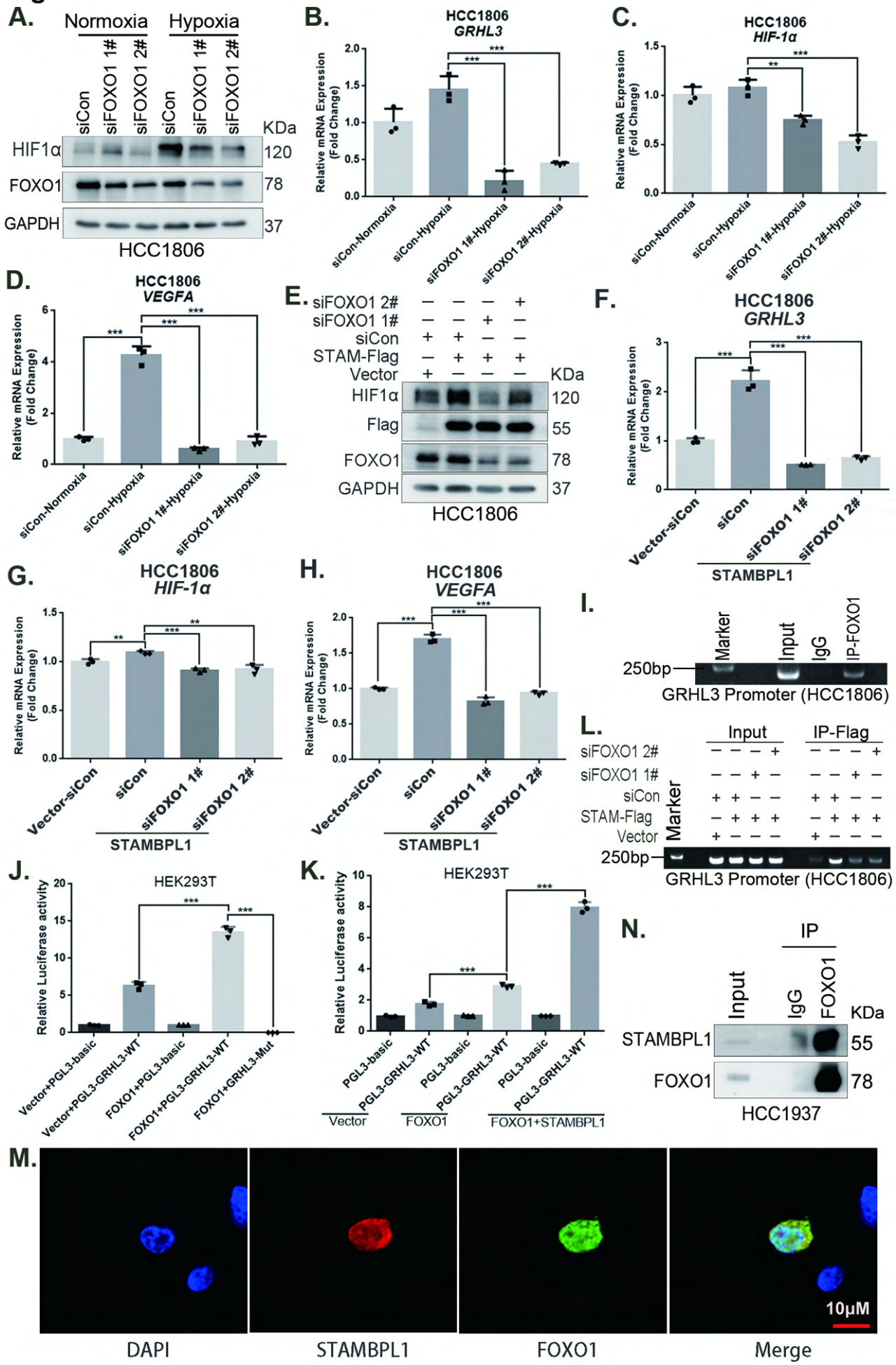
A.
Normoxia
Hypoxia
siCon
siFOXO1 1#
siFOXO1 2#
KDa
HIF1α
FOXO1
GAPDH
120
78
37
HCC1806
B.
HCC1806
GRHL3
Relative mRNA Expression (Fold Change)
siCon-Normoxia
siCon-Hypoxia
siFOXO1 1#-Hypoxia
siFOXO1 2#-Hypoxia
C.
HCC1806
HIF-1α
D.
HCC1806
VEGFA
E.
siFOXO1 2#
siFOXO1 1#
siCon
STAM-Flag
Vector
Flag
55
F.
HCC1806
GRHL3
Vector-siCon
STAMBPL1
G.
HCC1806
HIF-1α
H.
HCC1806
VEGFA
I.
Marker
Input
IgG
IP-FOXO1
250bp
GRHL3 Promoter (HCC1806)
L.
IP-Flag
J.
HEK293T
Relative Luciferase activity
Vector+PGL3-basic
Vector+PGL3-GRHL3-WT
FOXO1+PGL3-basic
FOXO1+PGL3-GRHL3-WT
FOXO1+GRHL3-Mut
K.
PGL3-basic
PGL3-GRHL3-WT
Vector
FOXO1
FOXO1+STAMBPL1
N.
IP
HCC1937
M.
10μM
DAPI
STAMBPL1
FOXO1
Merge

Figure 8

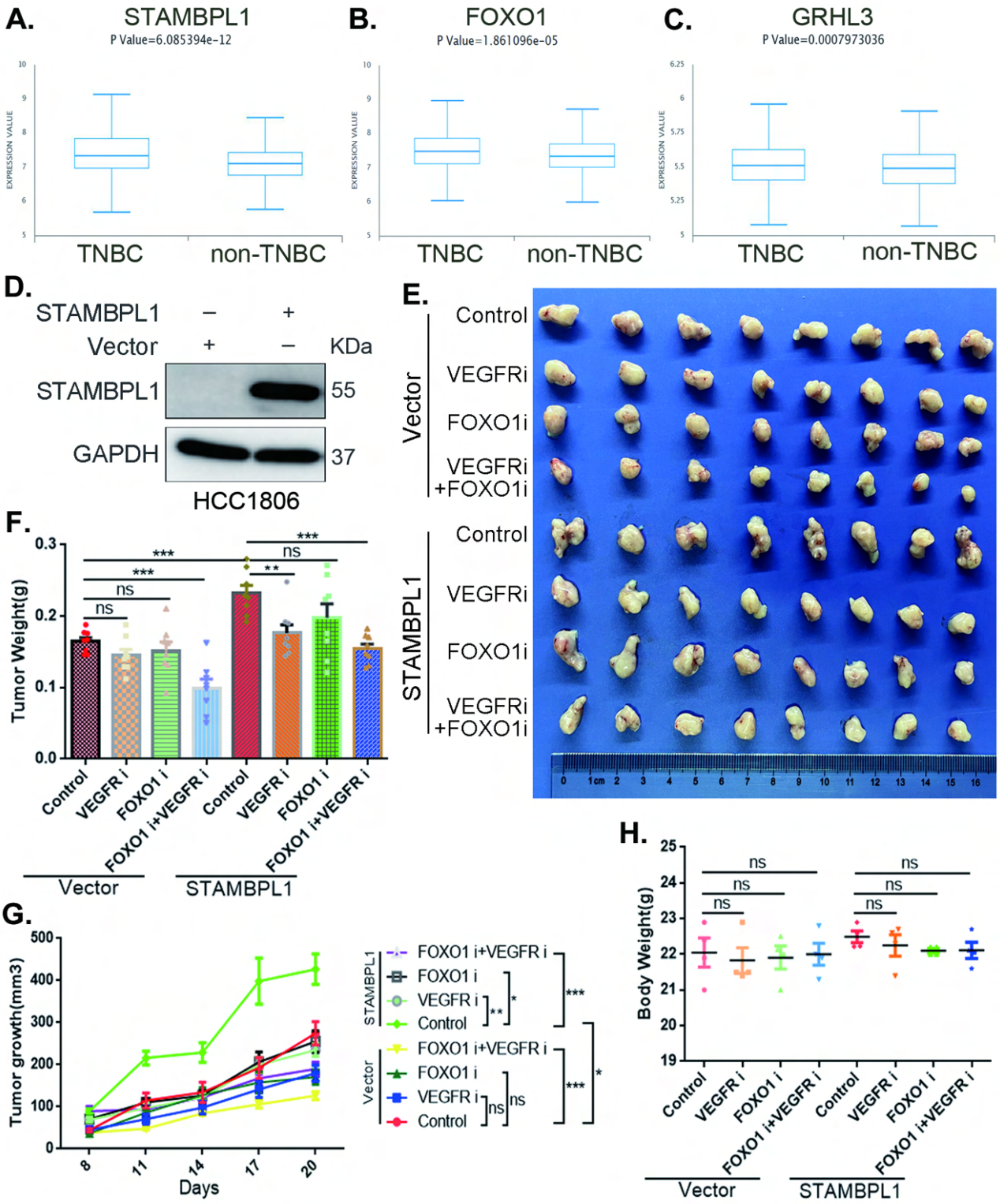
A.
STAMBPL1
P Value=6.085394e-12
EXPRESSION VALUE
TNBC
non-TNBC
B.
FOXO1
P Value=1.861096e-05
TNBC
non-TNBC
C.
GRHL3
P Value=0.0007973036
TNBC
non-TNBC
D.
STAMBPL1 – +
Vector + – KDa
STAMBPL1 55
GAPDH 37
HCC1806
E.
Vector
Control
VEGFRi
FOXO1i
VEGFRi +FOXO1i
STAMBPL1
Control
VEGFRi
FOXO1i
VEGFRi +FOXO1i
F.
Tumor Weight(g)
Control
VEGFR i
FOXO1 i
FOXO1 i+VEGFR i
Vector
STAMBPL1
G.
Tumor growth(mm3)
Days
STAMBPL1
FOXO1 i+VEGFR i
FOXO1 i
VEGFR i
Control
Vector
FOXO1 i+VEGFR i
FOXO1 i
VEGFR i
Control
H.
Body Weight(g)
Control
VEGFR i
FOXO1 i
FOXO1 i+VEGFR i
Vector
STAMBPL1

Figure 9

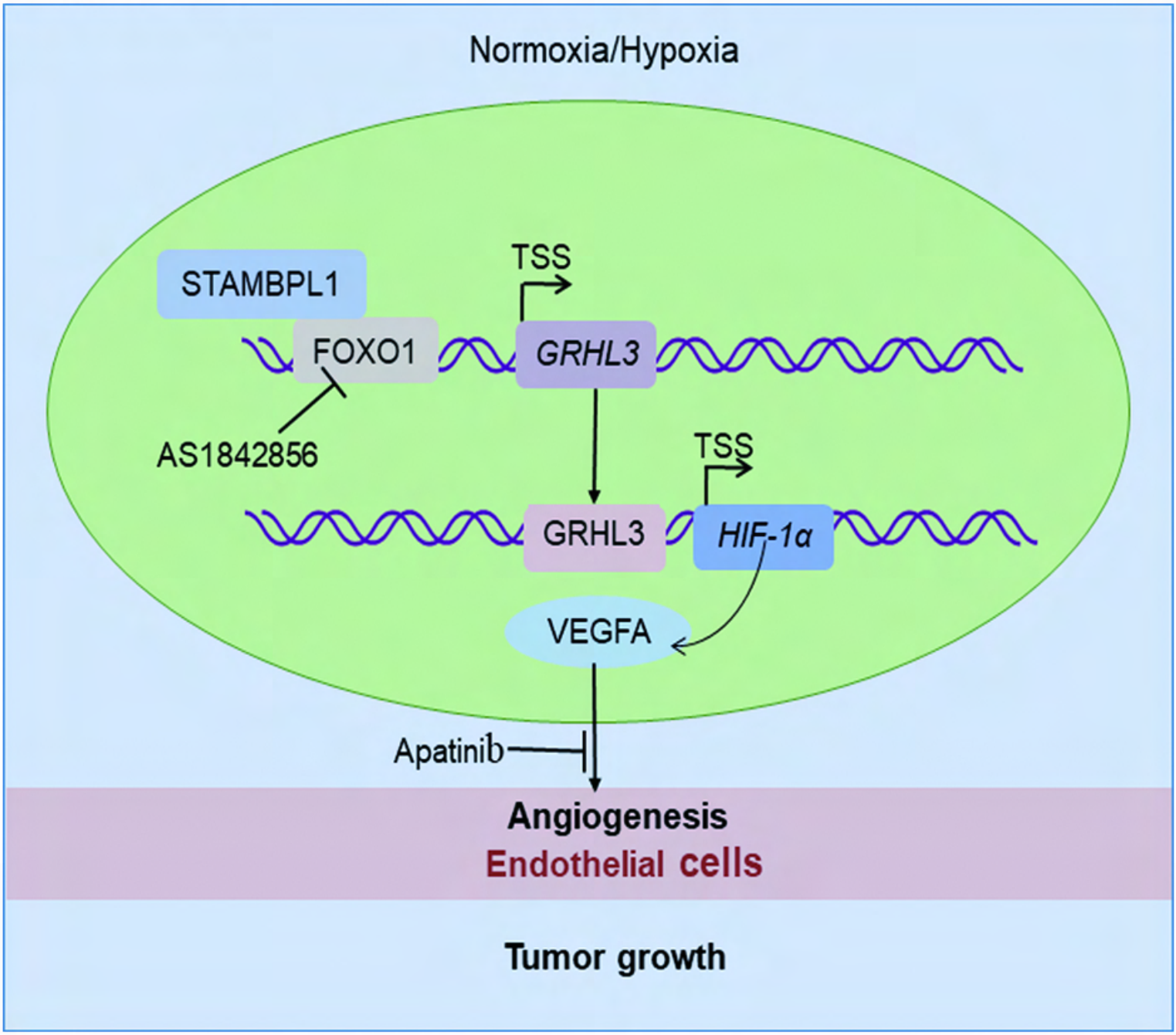
Normoxia/Hypoxia
STAMBPL1
TSS
FOXO1
GRHL3
AS1842856
TSS
GRHL3
HIF-1α
VEGFA
Apatinib
Angiogenesis
Endothelial cells
Tumor growth